MotorDoc LLC | HRI Labs

Technical Research Manuscript

Relating Motor Current Signatures to Mechanical Vibration

A frequency-resolved framework connecting spectral decibels with acceleration, velocity and displacement

Theory, worked calculations and an anonymized exploratory field comparison

EMPOWER MCSA and EMPOWER VIB
Current-feature processing reviewed against EMPOWER 3.1

12 September 2026 • Revised technical manuscript

Howard W. Penrose, Ph.D., CMRP

MotorDoc LLC and HRI Labs
Correspondence: info@motordoc.com

Manuscript status: exploratory study. Calculations have been checked; independent experimental validation and external peer review remain outstanding.

Table of Contents

Symbols and units

Symbols are grouped by their role in the equations. RMS means root mean square; RSS means root-sum-square; PSD means power spectral density. Subscripts identify the measured component, location or reference. Context-dependent symbols are distinguished below.

Signals and frequency

Symbol	Meaning	Unit
t; T_{rec}	Time; duration of a contiguous record.	s
f; $\omega = 2\pi f$	Frequency; angular frequency.	Hz; rad/s
f_s, f_c; f_r; f_m	Supply/carrier; component shaft; mechanical-feature frequency.	Hz
f_{samp}; f_k; Δf	Sampling frequency; frequency at bin k; bin spacing.	Hz
ω_r; $\Omega_{h,RMS}$	Rotor angular speed; RMS harmonic speed fluctuation.	rad/s
s; o	Induction-machine slip; mechanical order, f_m/f_r.	1
x, X; v, V; a, A	Displacement; velocity; acceleration. Lowercase: time/complex response. Uppercase: RMS.	m; m/s; m/s^2
X, V, A in field tables	Reported displacement, velocity and acceleration.	µm; mm/s; m/s^2
n; θ; a_n	Sensor unit-direction vector; angle to motion; projected acceleration.	1; rad; m/s^2
A_x, A_y, A_z; A_{RSS}	RMS acceleration by axis; root-sum-square of those components over the same interval.	m/s^2
i(t); I; v(t)	Instantaneous current; RMS current; voltage in electrical-power equations.	A; A; V
I_c; I_{sb}; I_{ref}; I_B	Carrier; single sideband; reference; band-integrated RMS current.	A
R, r(f); R_s; R_p; R_B	Normalized current ratio/complex response; single sideband; combined pair; band.	1
D, D_i, D_s, D_B, D_h, D_v	General/current/sideband/band/harmonic/vibration level. Each retains its stated reference.	dB
Q; m; q	Normalized mean-square ratio R^2; modulation index; common amplitude scale in Section 9.2.1.	1
q_j; H_{ij}; H_a; H_{nj}	Disturbance coordinate; gains to normalized current or acceleration.	By coordinate
H_h; S_e	Housing/gap displacement ratio; electrical sensitivity in the radial model.	1
G_{ie}; G_{he}	Torque-to-normalized-current gain; torque-to-housing-displacement gain.	$(N \cdot m)^{-1}$; $m/(N \cdot m)$
$S_i[k]$; $S_a[k]$	Current PSD; acceleration PSD.	A^2/Hz; $(m/s^2)^2/Hz$
w; NFFT; c(t)	Window weights; FFT length; centered converter counts in the calibration equation.	1; samples; counts

"1" denotes a dimensionless quantity. Angle values stated in degrees are marked explicitly. The voltage v(t) is distinct from mechanical velocity v; the window w is distinct from angular frequency ω.

Mechanical quantities and calculation symbols

Symbol	Meaning	Unit
F; F_x, F_y	Force; transverse components of net magnetic pull.	N
m, m_{eff}; k; c	Modal/effective mass; stiffness; viscous damping. This m is distinct from modulation index.	kg; N/m; N·s/m
g, g_0, δg; rg; l; Ag	Air gap/reference/perturbation; gap radius; active length; magnetic area.	m; m; m; m²
B, B_0; B_r, B_t; p_n, p_0	Flux density/reference; radial/tangential flux density; normal pressure/reference.	T; T; Pa
μ_0; $\mathcal{F}$; $\Re$; φ	Vacuum permeability; magnetomotive force; reluctance; circumferential angle.	H/m; A·turn; A·turn/Wb; rad
T_e; T_{shaft}; $T_{rot,loss}$; J	Air-gap electromagnetic torque; shaft torque; rotor mechanical-loss torque; rotor inertia.	N·m; kg·m² for J
T, T_h; M_f; n	Interface/harmonic torque; friction moment; rotational speed in friction-power equations.	N·m; N·m; r/min
$M_{rolling}$, $M_{sliding}$, M_{seal}, M_{drag}	Rolling, sliding, seal and lubricant-drag friction moments.	N·m
$G_{Ti,h}$; φ_h	Harmonic current-to-torque gain; torque–speed phase difference.	N·m/A; rad
P; P_{in}; $P_{friction}$; P_d; P_{mech}	Power; electrical input; friction loss; viscous dissipation; mechanical power.	W
P_{tol}; u_P	Specified watt tolerance; standard uncertainty of a power estimate. These are different quantities.	W
E_k; V_{rel}	Kinetic energy; relative RMS velocity across a dissipative interface.	J; m/s
P_{cu}; $R_{ac,h}$; $I_{ph,h}$	Copper loss; harmonic AC resistance; phase harmonic RMS current.	W; Ω; A
V_{ref}; K, K_a, K_v, $K_{v,e}$	Vibration reference; calibrated response gains. Gain units match the selected response per unit current ratio.	By response
n; e_i; J; $\theta = \ln K$	In fitting: sample count; log residual; objective function; log gain. Distinct from speed, inertia and angle.	1; stated units for K
K_{-i}; V_{predi}; F_i; b; u	Gain omitting motor i; predicted velocity; multiplicative error; fitted exponent; standard uncertainty.	By quantity; F_i and b: 1
y, y_0; L, L_0; α	Response/reference; archived estimated loss/reference; coefficient in $y^2 = \alpha L$.	By response; kW; y²/kW
i, j, k, h; B as index	Record/component/bin/harmonic indices; B labels an integration band, distinct from flux density.	1
h, r, t, 0, ref, est, pred	Subscripts: housing/harmonic, radial, tangential, baseline, reference, estimated, predicted.	—
Δ; δ; d; overbar; tilde; ⟨ ⟩	Change; small perturbation; differential; mean; zero-mean fluctuation; average.	By quantity
Σ; ∫; | |; j; ln; exp; $\log_{10}$	Sum; integral; magnitude; imaginary unit; natural logarithm; exponential; base-10 logarithm.	By operation

The calibration uses standard gravity 9.80665 m/s² per g. Multiply m/s by 10^3 for mm/s, m by 10^6 for µm, and kW by 10^3 for W. Numerical reproducibility tolerance is dimensionless; it is not a watt tolerance.

Abstract

A conversion from motor current signature analysis (MCSA) decibels to mechanical vibration requires more than a change of units. Current normalization, electromagnetic coupling, structural response and frequency weighting all enter the relationship. This paper derives a conditional model linking a current amplitude ratio R to vibration amplitude through a calibrated coefficient, $y \approx KR = K10^{D/20}$, and distinguishes it from exact acceleration–velocity–displacement conversions. A 2026 observational dataset contains 20 name-matched motors and 116 motor-side vibration recordings. An exploratory six-motor family comparison yields $V \approx 2.2094R$ for drive-end vertical velocity in the 1–2 kHz band, with V in mm/s RMS. The logarithmic correlation is 0.849. Coefficient-refitted omitted-motor predictions have median and worst error factors of 1.46 and 1.55, compared with 1.50 and 2.05 for a constant-response baseline. Normalization reverses the sign of the absolute-current association, and grouped checks show sensitivity to operating conditions. The result is a local calibration candidate, not a universal conversion. Mechanical condition affects both mean frictional demand and radial/torsional modulation; the paper develops condition-aware watt-loss estimates while distinguishing them from measured dissipation. The contribution is an auditable calculation framework and a testable hypothesis for synchronized validation.

Keywords: motor current signature analysis; vibration; spectral decibels; band RMS; electromechanical coupling; condition monitoring; calibration.

1 Research question and contribution

The primary question is whether a defined current-signature feature can estimate a defined vibration response with a simple, physically interpretable formula. The target is a quantitative amplitude relationship rather than fault classification alone. A useful answer must specify the current reference, frequency mapping, vibration units, sensor position and operating envelope.

Three levels of evidence are separated throughout: exact mathematical identities, conditional physical models and empirical field fits. The exact conversion $D \leftrightarrow R$ does not establish the coefficient K. The mechanical conversion between acceleration, velocity and displacement is exact for a resolved sinusoidal component, whereas a broadband conversion requires integration at each frequency. The field study tests whether a stable local coefficient is plausible; it does not identify a unique fault mechanism.

The theoretical contribution is the explicit chain from a mechanical disturbance to current modulation and measured vibration. The empirical contribution is a transparent, reproducible example with negative controls, baseline comparisons and operating-group sensitivity. These boundaries are essential to interpreting a simple formula responsibly.

2 Prior work and physical interpretation

Practical capability and acquisition recommendations in this manuscript give precedence to field applications, physical inspections and repair outcomes, particularly the supplied work of Howard W. Penrose [1], [2], [3], [4], [5], [6]. Those publications treat the machine air-gap magnetic field as the sensing element for radial AND torsional effects throughout the coupled system. Laboratory models [7], [8], [9], [10] provide supporting mathematical examples; their particular processing limits are not treated as limits of field MCSA.

Zhang et al. estimate an air-gap displacement profile from a quantitative electrical model and validate their approach experimentally [10]. This is an important precedent for quantitative electrical-to-mechanical inference. Air-gap displacement and accelerometer motion on a bearing housing are different coordinates, however. A transfer model is needed before interpreting one as the other. The present study takes a simpler empirical route and therefore makes narrower claims about transferability.

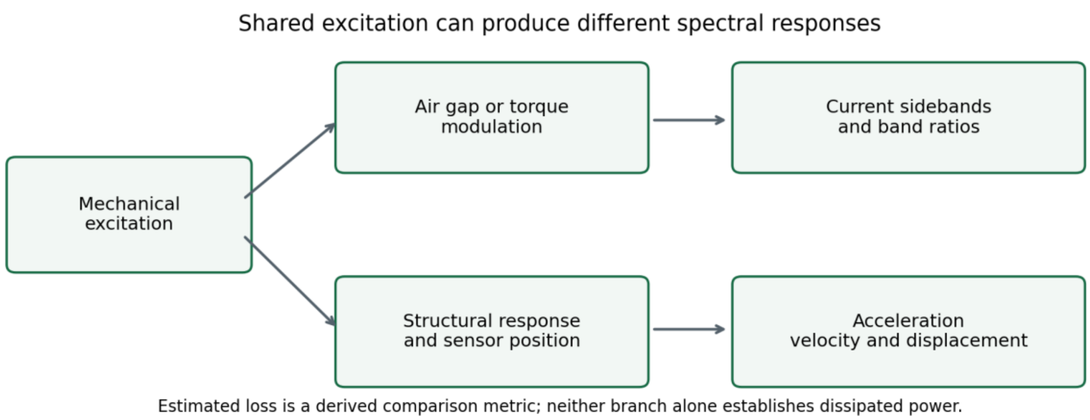

Figure 1. Conceptual coupling paths. Mechanical excitation can influence both current and vibration, but the electrical and structural paths have different gains and frequency responses.

2.1 Radial and torsional coupling

MCSA is sensitive to both radial and torsional influences. Radial effects include geometric gap variation and magnetic asymmetry; torsional effects include changes in air-gap electromagnetic torque and flux linkage associated with machine and driven-component condition [2], [4], [6]. Detectable shaft twist or speed variation is not a prerequisite. Horizontal, vertical and axial describe a vibration sensor's mechanical axis, whereas radial and torsional describe coupling mechanisms.

Let $q(f)$ describe one small mechanical disturbance at mechanical frequency f. For a linearized operating point, let the normalized electrical response be $r(f) = H_i(f)q(f)$, after the appropriate carrier demodulation, and let housing acceleration be $a(f) = H_a(f)q(f)$. The quantities are complex amplitudes in a consistent convention. If one disturbance dominates and H_i is nonzero, elimination of q gives

$$a(f) = [H_a(f)/H_i(f)]\, r(f); \quad |a(f)| = K_a(f)|r(f)| \quad (1)$$

K_a includes the sensor coordinate and operating point. Multiple disturbances, resonance, cancellation and independent noise can change the current-to-housing gain. A load change alone does not establish that the gain has changed. For a broadband relation $A \approx K_aR$, the weighted effective gain must also remain sufficiently stable across the compared records. Equal numerical band limits alone do not demonstrate this condition.

2.2 Directional response and system coverage

A single-axis accelerometer primarily measures the projection of local motion onto its sensitive axis. In an idealized model, a measured along unit vector n is $a_n = n \cdot a$. Mounting location, attachment stiffness and transverse sensitivity modify that response [11]. Horizontal, vertical and axial readings therefore describe different mechanical coordinates, not interchangeable samples of one scalar condition.

$$a_n = n \cdot a; \quad \text{for a linearly polarized component, } A_n = A|\cos\theta| \quad (2)$$

Direction example. A 1.00 m/s² RMS component aligned with a sensor reads 1.00 m/s². At 60° it reads 0.50 m/s²; at 90° an ideal single-axis sensor reads zero. Real transverse sensitivity and other motion prevent interpreting a small reading as proof of no disturbance. Three simultaneous orthogonal channels at one location can provide a direction-independent mean-square total $A_{rss} = \sqrt{(A_x^2 + A_y^2 + A_z^2)}$. Sequential measurements at different times or locations do not necessarily form that vector total.

MCSA is operationally omnidirectional: the current clamp has no horizontal, vertical or axial vibration sensing axis, and one acquisition contains radial and torsional information from the coupled system [4], [6]. Its sensing path is the air-gap magnetic response, rather than structural acceleration propagated to the clamp. It therefore provides system information without visiting each bearing. This does not make current a geometric vector sum of housing vibration; the quantitative coordinate conversion still requires a transfer relationship.

$$r(f) = \Sigma_j H_{ij}(f)q_j(f); \quad a_n(f) = \Sigma_j H_{nj}(f)q_j(f) \quad (3)$$

Equation 3 generalizes Equation 1 to multiple disturbance coordinates. The coefficients can differ in magnitude and phase; contributions can reinforce or cancel. One current feature cannot uniquely reconstruct three vibration directions without additional measurements or model constraints. Phase-current channels are electrical phases, not mechanical axes. A per-position coefficient K_n is therefore expected even when all positions share the same current feature.

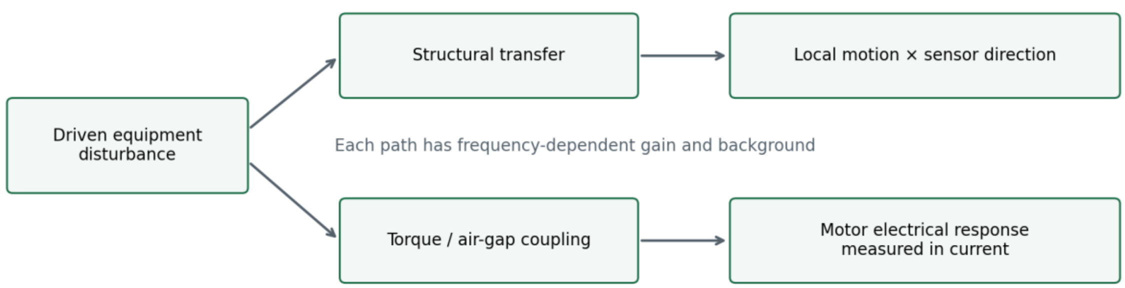

Figure 2. Measurement coverage follows transfer paths. Vibration observes motion through the structure and the sensor axis; current observes disturbances transmitted into the motor's electrical response. The diagram specifies paths, not a detection distance.

2.2.1 Transducer placement and loss of diagnostic contrast

A vibration reading belongs to a location, direction and mounting condition. For a bearing assessment, use a rigid part of the bearing housing with a short structural path to the bearing; an accessible cover, cooling fin or remote support may represent a different response. Mark the position and orientation so subsequent measurements reproduce the same coordinate [11], [12], [13].

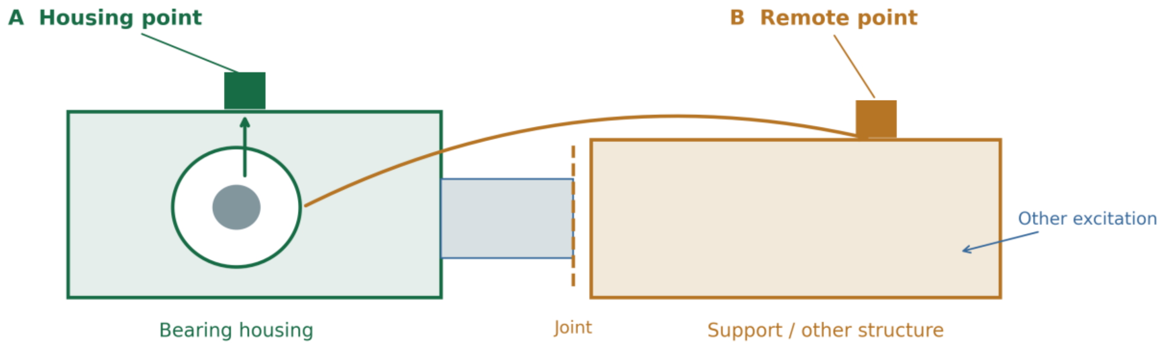

Figure 3. Schematic placement comparison. A short bearing-to-sensor path and a remote path through a joint sample different structural responses. The remote signal can be attenuated, amplified or mixed with other sources. Arrow lengths are schematic, not measured amplitudes.

How a feature is weakened or obscured	Effect on the reading and practical control
Axis misalignment	Projection reduces the measured component: at 60°, an ideal single-axis reading is half the aligned value. Record the axis and retain directional spectra.
Compliant or inconsistent mounting	Soft interfaces and added mounting mass alter the usable frequency response. Use a prepared surface and a mount qualified for the required band [12].
Long or interrupted structural path	Joints and local modes change transmission; another source can dominate. Choose the bearing housing for bearing response, rather than assuming a remote point is equivalent [11], [13].
Sensor or mount resonance	A peak can be amplified as well as attenuated. Check the installed sensor/mount bandwidth; do not apply a universal correction factor [12].
Broadband or cross-axis averaging	A small defect feature may be hidden by unrelated energy. Preserve the individual waveforms, spectra, axes and relevant bands before forming a summary.

Here "dilution" means reduced diagnostic contrast, not necessarily less total RMS. A resonant cover can produce a larger overall value while making bearing interpretation worse. Poor attachment may also create false impacts. These structural-path effects are distinct from MCSA's radial and air-gap torque sensing; they must not be imposed as restrictions on calculated-current-peak diagnosis.

2.2.2 Single-axis and triaxial vibration measurements

A linear single-axis accelerometer measures translational acceleration along one sensitive axis. A triaxial accelerometer measures three approximately orthogonal translational components at one location. “Linear” does not mean that triaxial sensing is nonlinear, and a triaxial unit is not a direct shaft-torsion sensor. The acquisition system must support simultaneous channels to obtain the timing benefit [13].

Comparison	Single-axis	Triaxial
Directional information	One component per orientation; repositioning is needed for other axes.	Three local components; map sensor axes to machine horizontal, vertical and axial directions.
Location equivalence	Measurements on the top and side of a housing follow different paths.	The horizontal channel of a top-mounted unit need not equal a side-mounted radial reading [13].
High-frequency response	Depends on sensor, mount and path for the chosen coordinate.	Check each axis and its installed bandwidth; three axes do not remove mounting or structural filtering.
Motion and timing	Sequential readings can sample different states during changing operation.	Simultaneous channels capture the same interval. Local rocking may affect one position more than another [13].
Coverage and route time	One sensor may serve many prepared points, with repeated positioning.	One attachment can acquire three axes at a site; other bearings still need their own measurement sites.

Combining axes can obscure a feature

Consider a calculated example with RMS components $A_x = 1.00$, $A_y = 0$ and $A_z = 0$ m/s². Their arithmetic average is 0.333 m/s², 9.54 dB below the active-axis amplitude; dividing summed mean squares by three and taking the root gives 0.577 m/s², 4.77 dB lower. Neither is the total vector RMS. The appropriate unweighted total over the same interval is $A_{RSS} = \sqrt{(A_x^2 + A_y^2 + A_z^2)} = 1.00$ m/s². Triaxial sensing itself has not diluted this signal; the summary calculation has changed the quantity.

Even a correct RSS can hide a directional change: if one axis rises from 0.10 to 0.20 m/s² while the other two stay at 1.00 m/s² each, that axis doubles, but total RMS rises only from 1.418 to 1.428 m/s², about 0.74%. Conversely, directly adding signed waveforms from different axes can cancel components. Taking an FFT of instantaneous vector magnitude is nonlinear and does not preserve the original axis spectra. Keep axis-specific features alongside any overall total.

A calibrated triaxial measurement can provide stronger local directional evidence with fewer attachments. It cannot recover a vibration feature already lost in the path to that location. For the current-to-vibration relationship, define whether the target is one axis or a simultaneous RSS; a coefficient fitted to one must not be transferred to the other unchanged.

2.3 How far into the system can each method see

Neither method has a fixed reach in meters or a fixed number of connected components. Detectability depends on the disturbance amplitude, frequency-dependent path gain and measurement background. Electrical access at a remote motor feeder is also different from mechanical reach into the driven equipment: moving the current measurement point does not create coupling to a mechanically invisible disturbance.

Aspect	Vibration measurement	MCSA
Primary path	Force or motion through bearings, housings, supports, couplings and foundations.	Radial magnetic effects and small air-gap torque changes represented in current.
Local sensitivity	Often strong near a source with a short, rigid path; direction and mounting matter.	Can detect motor electrical or coupled mechanical effects without placing a sensor at the fault.
Driven-system reach	Can receive remote structural vibration; joints, isolation, modes and mounting alter it.	Field applications identify gearbox, main-shaft bearing and blade-related conditions from one electrical point [4], [6].
Frequency limitations	Path attenuation, resonances, antiresonances and sensor bandwidth determine visibility.	Carrier mapping, record processing, magnetic/electrical response and spectral separation determine visibility.
Localization	Multiple locations and directions help distinguish a local source and transmission path.	An integrated response can be ambiguous; similar torque modulations may have different sources.

Vibration guidance favors a short rigid path between the source and sensor [11]. Joints, damping and structural modes can attenuate or amplify high-frequency bearing impacts. MCSA bearing analysis instead examines the radial or torsional influence on the air-gap field, including small frictional and torque changes. It does not require the high-frequency housing vibration waveform to propagate intact through the shaft train. Penrose reports main-bearing and gearbox condition from generator electrical measurements [4], [6].

Reference [14] examines gearbox detection using motor-current and vibration-related processing. Its reported difficulty with high-frequency vibration signatures is specific to that approach. Applying vibration high-frequency detection assumptions to MCSA bearing analysis conflates two sensing paths. It is not a basis for restricting downstream bearing capability. The field evidence in [4], [6] takes precedence for the practical scope addressed here.

$$\text{Detectable response requires } |H(f)q(f)| \text{ to exceed the relevant background} \quad (4)$$

Equation 4 refers to the electrical response to a radial or air-gap torque disturbance, not a requirement for measurable shaft-speed variation. In a DFIG field case, Penrose reports increasing air-gap torque oscillation with load while mechanical RPM remains constant [30, Section V]. A rotor-inertia speed-ripple model alone therefore cannot define MCSA sensitivity or system reach. Small changes in electromagnetic torque can appear in current without a shaft-speed instrument resolving a change.

Consequence for the proposed formula. Calibrate each vibration coordinate separately, or predefine a simultaneous three-axis total. Include coupling type, driven machine, operating condition and measurement location in the validity envelope. A current-based estimate may provide broad system surveillance while directed vibration measurements help locate the source. This dataset does not establish a measured detection distance or omnidirectional vibration reconstruction.

2.4 Prior research and publication

Six supplied full papers were reviewed. The field observations below provide the principal basis for the diagnostic scope and workflow. Where a result uses voltage and current ESA, that measurement configuration is retained.

Field source	Observation and confirmation	Consequence for this manuscript
Penrose, 2015 insulation forensics [3]	Thirteen failed generators were reviewed; eleven underwent the winding-failure investigation. Coil looseness, packing and wedge debris formed a proposed failure chain.	Mechanical condition and electrical insulation degradation can be related. This is forensic evidence, not a detection-rate study.
Penrose, 2020 interturn stress [1]	VFD tuning/filter changes reduced signatures; selected DFIG stator and rotor indications were checked by surge testing.	Interpret developing stress before a dead short. DFIG stator evidence was primarily voltage: retain the ESA distinction.
Penrose, 2021 wedges/coils [5]	Slot-related signatures were associated with inspected coil or wedge conditions; pre/post-repair ESA supported mitigation.	Magnetic changes can be detectable without a corresponding measurable static-eccentricity response.
Penrose, 2022 system interactions [2]	Field assessment links generator, drivetrain, converter and transformer behavior; air-gap torque oscillated at constant mechanical RPM.	Air-gap torque is distinct from measured shaft-speed ripple. Full ESA supports broader electrical-system analysis.
Penrose, practical DFIG application [4] and 2025 PES paper [6]	Describe bearings, gears, main bearings, rotor connections and wedges; [6] specifies one-phase, 120-second MCSA.	Use one CT and one acquisition for simultaneous coupled-system diagnosis. Target vibration measurements to the identified mechanical question.

These field reports support practical diagnostic capability. They do not identify the coefficient converting a current feature into housing velocity at a specified location. The present regression addresses that separate quantitative question.

Operation under changing load speed and frequency

MCSA can identify issues in equipment whose load, speed and electrical frequency change. Evaluate the calculated component peaks and their carrier-relative dB values at the applicable frequencies; equal-load comparisons are not a prerequisite for this diagnostic method [4], [6], [15]. Speed or frequency changes relocate calculated signatures, rather than making the technology inapplicable. Matching operating states is often useful in vibration-amplitude comparison and in this paper’s quantitative housing-response study; it must not be imposed as a routine MCSA diagnostic rule.

Practical lower-load limits depend on the resolution available to separate the relevant calculated peaks, not a universal minimum percentage of rated load. For an induction-motor rotor example, sideband separation is $2sf_s$, where s is slip: as slip decreases, the sidebands approach the carrier. Finer effective resolution extends separation at lower slip. Window width, carrier background and frequency movement enter the actual separation test. This example does not impose a slip-based limit on every bearing, stator or driven-component signature [6], [15].

2.5 Material transmission and magnetic coupling

Structural transmission

Vibration propagates through the elastic structure as coupled motion and stress, with joints, supports and material damping affecting the response. A single-mode approximation illustrates the frequency dependence. If F is harmonic force and x_h is housing displacement,

$$x_h(\omega)/F(\omega) = 1/[k - m\omega^2 + jc\omega]; \quad a_h(\omega) = -\omega^2 x_h(\omega) \quad (5)$$

m, c and k are modal mass, damping and stiffness, not necessarily the total motor mass or static support stiffness. In a real structure, mode shapes at the source and sensor multiply each modal contribution. Resonances, nodes and antiresonances can make the same force produce very different directional readings. This model explains path effects; it is not an identified model of the tested motors [11], [16].

Magnetic coupling across the air gap

For a simplified unsaturated magnetic circuit dominated by one effective air gap, reluctance $\mathfrak{R} \approx g/(\mu_o A g)$ and flux density $B \approx \mu_o \mathcal{F}/g$, where $\mathcal{F}$ is magnetomotive force. At fixed $\mathcal{F}$, a small radial gap perturbation gives

$$\Delta B/B_o \approx -\Delta g/g_o; \quad p_n \approx B^2/(2\mu_o); \quad \Delta p_n/p_o \approx 2\Delta B/B_o \quad (6)$$

The pressure expression assumes predominantly normal flux and follows magnetic-energy/Maxwell-stress reasoning [17]. In a motor, distributed fields, saturation, slotting and electrical feedback complicate this local approximation. An illustrative 1% gap increase at fixed magnetomotive force reduces local flux density by approximately 1% and magnetic pressure by approximately 2%. It does not imply a 1% change in line current or housing vibration.

An explicit conditional bridge

Let δg be a resolved RMS radial gap variation, R_s a corresponding normalized current feature, S_e its dimensionless electrical sensitivity, and H_h the housing-displacement/gap-displacement transfer ratio. Then $R_s \approx |S_e|\delta g/g_o$ and $X_h \approx |H_h|\delta g$. Eliminating δg gives

$$V_h \approx 10^3 \omega g_o \, |H_h/S_e| \, R_s \quad [\text{mm/s RMS}] \quad (7)$$

$$K_v(\omega) = 10^3 \omega g_o \, |H_h/S_e|; \quad V_h \approx K_v(\omega) 10^{D_s/20} \quad (8)$$

Illustrative radial calculation. Assume g_o = 0.500 mm, δg = 5.00 µm RMS, $|S_e|$ = 2 and $|H_h|$ = 0.20 at 30 Hz. Then R_s = 2 × 5/500 = 0.0200, D_s = −33.9794 dB, and X_h = 1.00 µm RMS. The predicted housing velocity is 0.188496 mm/s RMS. These chosen parameters demonstrate the calculation; they were not identified for the field motors.

This derivation supplies a physical interpretation of K without pretending that it is known. S_e must include the chosen sideband or demodulation convention, and H_h includes location and direction. Zhang et al.'s model-based gap reconstruction supports the need for electrical identification [10]. The empirical broadband coefficient in Section 7 is an effective calibration and has not separately identified g_o, H_h or S_e. For torque-driven mechanisms a torque-to-current and torque-to-motion model must replace this radial-gap example.

2.5.1 Unbalanced magnetic pull and the ESA and MCSA relationship

Unbalanced magnetic pull (UMP) is the net radial electromagnetic force that remains when magnetic stresses around the air gap do not balance. It connects magnetic-field asymmetry, rotor and bearing loading, and the vibration transmitted to a housing. ESA and MCSA observe the associated electrical response through changes in flux linkage and current modulation. Thus UMP provides a physical connection between the methods, while each measures a different response [5], [18], [19].

For the radial-pressure approximation of Section 2.5, the two transverse components of net pull are obtained by integrating the pressure around the gap:

$$F_x(t) \approx l r_g \int_0^{2\pi} p_n(\varphi,t) \cos \varphi \, d\varphi; \quad F_y(t) \approx l r_g \int_0^{2\pi} p_n(\varphi,t) \sin \varphi \, d\varphi$$

F_x and F_y are orthogonal force components in newtons; l is active length, rg is gap radius, φ is circumferential angle and p_n is radial magnetic pressure in pascals. This cylindrical approximation omits end effects and the transverse contribution of tangential stress. Uniform pressure gives zero net pull even though local magnetic pressure is nonzero. The spatial distribution, not simply the mean field magnitude, determines UMP.

Magnetic asymmetry and the measured mechanical response

Penrose distinguishes the magnetic position represented by an eccentricity signature from an assumed physical rotor displacement [18]. A stator-fixed asymmetry and an asymmetry rotating with the rotor have different spectral patterns. Electrical or magnetic asymmetry can therefore produce diagnostic evidence without the geometrical rotor movement implied by a simple eccentric-shaft drawing. Bearings and the shaft respond to the net force according to their stiffness and dynamics; the housing and sensor mount then impose further directional transfer effects.

At a vibration transducer, the UMP-driven response depends on the force direction, measurement axis, bearing load path, housing modes and attachment. A single-axis sensor can under-represent motion nearly perpendicular to its sensitive axis. A triaxial sensor resolves three local translational components, but neither removes structural attenuation nor measures every bearing location. UMP can also alter bearing loading and interact with mechanical excitation. Consequently, a vibration amplitude change cannot by itself quantify UMP or uniquely identify its cause.

Prior research and publication

The supplied 2021 field paper reports that small changes from stator wedge loss or coil movement can change the magnetic field without producing sufficient UMP for a measurable static-eccentricity indication [5]. Its inspected and repaired cases support electrical diagnosis beyond a requirement for strong mechanical vibration. The supplied DFIG powertrain work extends the practical interpretation to coupled components and to both radial and torsional signatures [4], [6].

Huang et al. model bidirectional coupling: bearing-related motion changes gap permeance and current, while magnetic pull feeds back into rotor motion. Their simulation and laboratory comparisons illustrate why current and vibration can contain related fault modulation [19]. This supports the mechanism; its test conditions do not define field detection limits or take precedence over the supplied field evidence.

UMP is the radial-force branch of the relationship. Air-gap torque is the tangential-stress branch developed next. Current signatures can reflect either or both; neither a large UMP nor measurable shaft-speed ripple is a prerequisite for every ESA/MCSA diagnosis. Identifying related calculated peaks does not require equal amplitudes or identical raw frequencies in the electrical and vibration spectra. The conversion coefficient must retain the mechanism, frequency and vibration location/direction.

2.6 Air-gap torque and the torsional current relationship

Air-gap torque is electromagnetic torque developed by field interaction; it is not necessarily the torque measurable at a shaft location. In a cylindrical air-gap approximation, tangential Maxwell stress is $B_r B_t/\mu_o$. Integrating stress times radius gives the following model, where l is active length, rg gap radius and φ circumferential angle [17]. End effects are omitted.

$$T_e(t) = (l r_g^2/\mu_o) \int_o^{2\pi} B_r(\varphi,t) B_t(\varphi,t)\, d\varphi \quad (9)$$

The small-signal variation is $\delta T_e \approx (l r_g^2/\mu_o)\int(B_{ro}\delta B_t + B_{to}\delta B_r)d\varphi$. Thus small changes in the field components change electromagnetic torque. Geometric radial motion is one possible cause; torque-related flux changes do not require a measurable change in physical radial clearance. These stress equations are an explanatory model, not a claim that a single CT directly measures the entire field.

$$J\, d\omega_r/dt = T_e - T_{shaft} - T_{rot,loss} \quad (10)$$

Equation 10 uses a motor-positive lumped rotor balance: J is inertia, ω_r shaft angular speed and $T_{rot,loss}$ rotor mechanical-loss torque. A shaft sensor measures torque at its own cross-section. Even at constant speed, electromagnetic torque and shaft torque need not be equal because of losses. Perturbations can balance while measured RPM remains unchanged, as reported in the field case [2]. MCSA detection therefore does not require measurable shaft acceleration or shaft-torque ripple.

Conditional bridge to measured housing vibration

For one identified torque-related disturbance, define G_{ie} as normalized-current response per air-gap torque perturbation and G_{he} as housing displacement per the same perturbation. These are effective, frequency-dependent transfer functions; they are not obtained from dB alone. With $\omega_m = 2\pi f_m$,

$$R_s = |G_{ie}\delta T_e|; \quad X_h = |G_{he}\delta T_e|; \quad K_{v,e} = 10^3\omega_m |G_{he}/G_{ie}| \quad (11)$$

$$V_h \approx K_{v,e} 10^{D_s/20}; \quad A_h = \omega_m V_h/10^3; \quad X_h = V_h/(10^3\omega_m) \quad (12)$$

V_h is mm/s RMS, A_h is m/s² RMS and X_h is m RMS. For illustrative $|G_{ie}| = 0.20\ (\text{N·m})^{-1}$, $|G_{he}| = 2.0$ µm/(N·m), $f_m = 15$ Hz and $R_s = 0.001$ (−60 dB), the inferred torque amplitude is 0.005 N·m and housing displacement 0.010 µm. $K_{v,e} = 0.942478$ mm/s and $V_h = 0.000942478$ mm/s. These assumed gains demonstrate the calculation; they are not measured sensitivities or detection thresholds.

The radial bridge in Section 2.5 and this torsional bridge explain why the same simple form can apply with different coefficients. Current can diagnose a torque-related condition even when housing response is very small. A small measured vibration response does not invalidate the electrical finding, and diagnostic capability does not establish a universal vibration-amplitude conversion.

2.7 Visual guide to the two coupling mechanisms

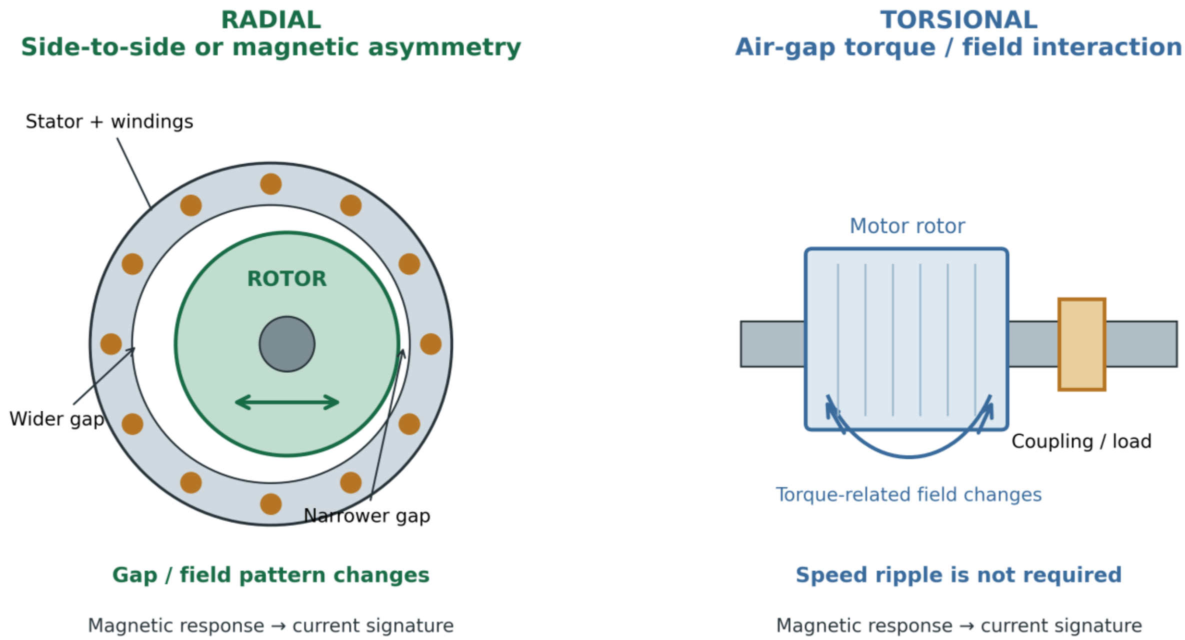

Figure 4. Radial and torsional mechanisms, illustrated schematically. Left: an exaggerated physical gap change; magnetic asymmetry can also occur without the same rotor movement. Right: torque-related interaction through the air-gap field. Measurable shaft-speed ripple is not required. Both mechanisms can modulate current. These are explanatory drawings, not measured defects.

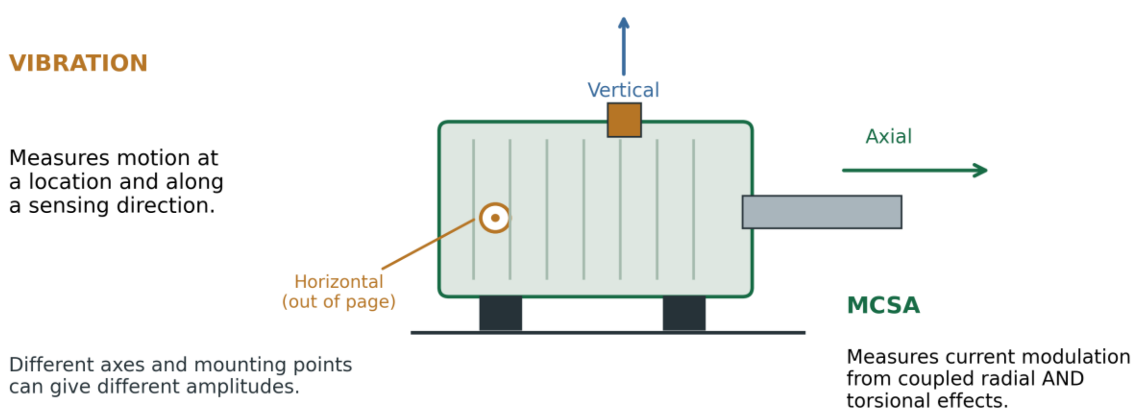

Figure 5. Measurement direction for a horizontal-shaft motor. The dot-in-circle denotes motion out of the page. A vibration sensor measures a selected local component; MCSA integrates radial and torsional effects that couple into the electrical response. Arrows describe axes, not measured amplitudes.

The physical question is different for each instrument. Vibration asks how this part of the structure moves in this direction. MCSA asks how the disturbance changes current through the motor's electromagnetic response. A calibrated transfer coefficient connects the answers only within its stated conditions.

3 From current sidebands to a mechanical frequency

3.1 Amplitude modulation example

For an ideal carrier at supply frequency f_s amplitude-modulated by one mechanical frequency f_m, write the current as Equation 13. I_c is carrier RMS current and m is the dimensionless modulation index. This illustrative signal is not a fitted model of the field records.

$$i(t) = \sqrt{2}\, I_c\, [1 + m \cos(2\pi f_m t)] \cos(2\pi f_s t) \quad (13)$$

Using $\cos\alpha \cos\beta = ½[\cos(\alpha + \beta) + \cos(\alpha - \beta)]$, each sideband has RMS magnitude $mI_c/2$. Thus a single-sideband ratio $R_s = I_{sb}/I_c$ gives $m = 2R_s$. If both sidebands are combined by root-sum-square, their ratio is $R_p = m/\sqrt{2}$. A coefficient fitted to R_s must not be applied to R_p unchanged.

$$D_s = 20 \log_{10}(R_s); \quad R_s = 10^{D_s/20}; \quad m = 2 \times 10^{D_s/20} \quad (14)$$

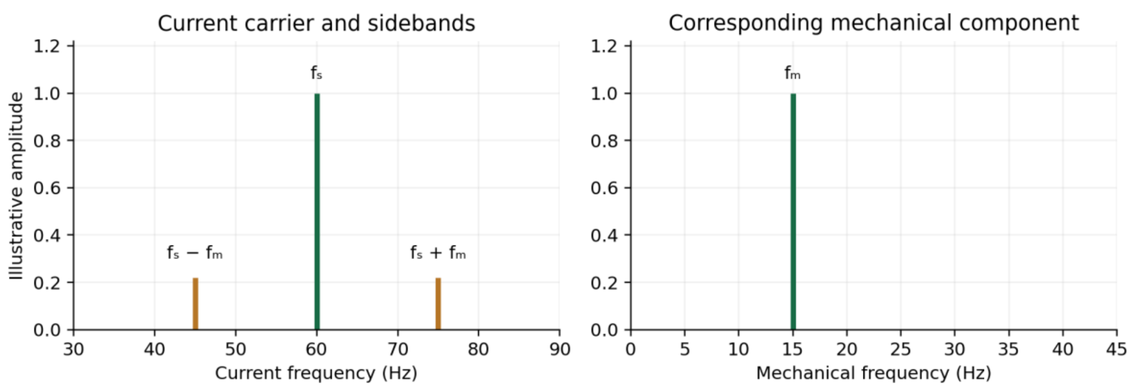

Figure 6. Illustrative mapping: a 15 Hz modulation of a 60 Hz carrier produces 45 and 75 Hz sidebands. Mechanical and electrical frequencies must be paired through a model.

Worked example. For I_c = 50 A RMS and one sideband at −40 dB relative to that carrier, $R_s = 10^{-2}$ = 0.01, I_{sb} = 0.50 A RMS and m = 0.02. Both sidebands combined give 0.7071 A RMS and −36.9897 dB. None of these values alone specifies housing vibration: K_a or a mechanical transfer model is still required.

3.2 What changes in a real motor

Torque modulation can produce phase modulation, and multiple supply harmonics can carry translated signatures [7], [8]. Consequently, the amplitude-modulation example supplies a calculation convention, not a universal diagnostic model. Leakage near a strong component can also bias a weak signature [20]. Acquisition-comb interpolation and spectral-leakage control address distinct problems. The field band fit later in this paper uses integrated band ratios, not an identified pair of mechanical sidebands.

4 Exact vibration and decibel calculations

4.1 Resolved sinusoidal motion

For $x(t) = \sqrt{2}\, X \cos(2\pi ft)$, X denotes displacement RMS. Differentiation gives velocity and acceleration RMS; the phase changes do not alter these magnitude identities. With $\omega = 2\pi f$,

$$V = \omega X; \quad A = \omega V = \omega^2 X; \quad V = A/\omega; \quad X = A/\omega^2 \quad (15)$$

Worked example. At 30 Hz, ω = 188.4956 rad/s. An acceleration of 1.000 m/s² RMS corresponds to V = 0.0053052 m/s = 5.3052 mm/s RMS and X = 0.0000281448 m = 28.1448 µm RMS. Peak displacement is √2X = 39.8027 µm; peak-to-peak displacement is 2√2X = 79.6054 µm. Mixing these conventions introduces fixed factors unrelated to motor behavior.

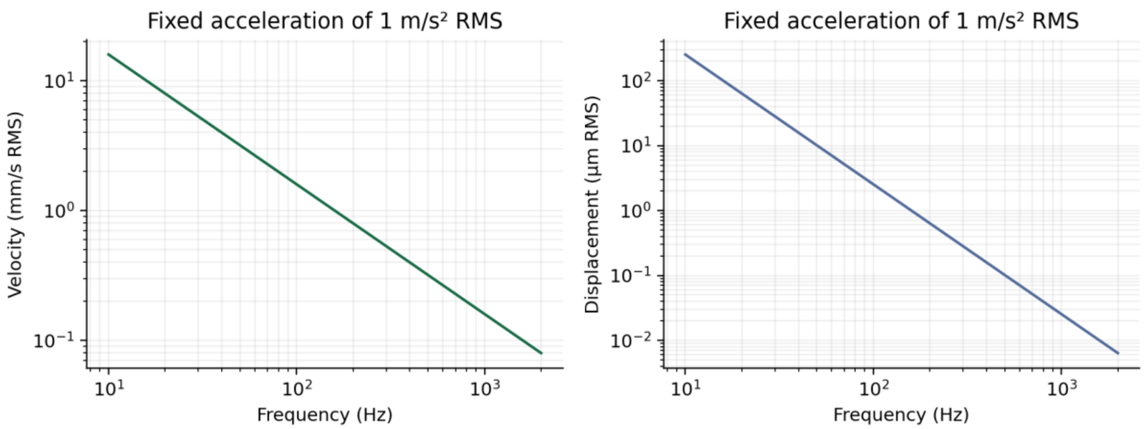

Figure 7. Exact sinusoidal conversions for fixed acceleration. Velocity falls as 1/f and displacement as 1/f². These curves are theoretical, not measured motor trends.

4.2 Decibels retain their reference

$$D_i = 20 \log_{10}(I/I_{ref}); \quad I = I_{ref} 10^{D_i/20} \quad (16)$$

The reference must be recorded with every dB result. A relative current level is dimensionless and is not interchangeable with dB re 1 A or with a vibration level referenced to acceleration, velocity or displacement. For D = −40 dB, the amplitude ratio is 0.01 and the mean-square ratio is 0.0001, or 0.01%. The same decibel value can therefore represent different absolute current at different loads.

$$Q = R^2 = 10^{D/10}; \quad D_v = D_i + 20 \log_{10}(K_v/V_{ref}) \quad (17)$$

The second identity assumes $V = K_v R$ and $D_v = 20 \log_{10}(V/V_{ref})$. K_v and V_{ref} must use identical units. A +6.0206 dB change doubles predicted amplitude only while the model coefficient and reference definition remain applicable.

5 Broadband calculations and measurement method

5.1 Integrate power density before taking a square root

For the independent research band-energy calculation, a conventional one-sided periodogram at an interior bin is $S[k] = 2|FFT(wx)[k]|^2/(f_{samp}\Sigma w^2)$. Welch PSD averages these power estimates. DC and Nyquist are not doubled; S has squared-amplitude/Hz units. These are standard research calculations [21], not a disclosure of EMPOWER's proprietary processing. MCSA systems need not use Welch; it must not be assumed to describe EMPOWER's diagnostic method. Zero padding refines the grid but not independent resolving power.

$$I_B = \sqrt{[\Sigma_B S_i[k]\Delta f]}; \quad R_B = I_B/I_{ref}; \quad D_B = 20 \log_{10} R_B \quad (18)$$

$$A_B = \sqrt{[\Sigma_B S_a[k]\Delta f]} \quad (19)$$

$$V_B = 10^3 \sqrt{[\Sigma_B S_a[k]\Delta f/(2\pi f_k)^2]} \quad [\text{mm/s RMS}] \quad (20)$$

$$X_B = 10^6 \sqrt{[\Sigma_B S_a[k]\Delta f/(2\pi f_k)^4]} \quad [\mu\text{m RMS}] \quad (21)$$

Here S_a is in $(m/s^2)^2$/Hz, and the sums include lower band edges and exclude upper edges. Frequencies at zero are excluded from integration to velocity and displacement. For disjoint bands, mean squares add; RMS amplitudes do not. Overlapping bands such as 10–1,000 Hz and its constituent bands must not be added together.

5.2 Why a single broadband conversion frequency fails

Consider two resolved components, each 0.100 m/s^2 RMS, at 30 and 300 Hz. Total acceleration is $\sqrt{(0.1^2 + 0.1^2)} = 0.141421$ m/s^2. Their velocities are 0.530516 and 0.053052 mm/s, so total velocity is 0.533162 mm/s. Converting total acceleration at an arbitrary 165 Hz instead gives only 0.136412 mm/s. The discrepancy comes from frequency weighting, not calibration error.

5.3 Vibration calibration used in this study

$$a(t) = [c(t)/(805863 \times 1.00329051 \times 0.100)] \times 9.80665 \quad (22)$$

c(t) denotes centered ADC counts, 805863 is counts/V, 1.00329051 is the implemented 44.1 kHz correction, and 0.100 is sensor sensitivity in V/g. Floating-point PCM samples are first converted to counts using 2^{23}. Equation 22 precedes the implemented 0.5 Hz high-pass filtering. As a scale check, 80586.3 counts corresponds to 0.996720 g or 9.77449 m/s^2 before filtering. The selected calibration is not an independent certification of the acquisition chain.

6 Field design and processing controls

The observational inventory contains 20 motors matched by acquisition identity and 116 motor-side vibration recordings collected in 2026. Repeated recordings for a motor, position and feature were reduced to a median. The motor is the analysis unit; repeated recordings are not additional independent motors. Family A comprises six motors and Family B four. The principal direct-current example uses A1–A6. Current and vibration for A1–A3 were recorded on different days; the other three were recorded on the same day but were not established as simultaneous.

Item	Implemented definition
Current reference	Largest corrected RMS spectral component in 0–5 kHz; near 60 Hz for these records.
Diagnostic application	EMPOWER 3.1 provides calculated-peak condition evaluation. Proprietary implementation is outside this manuscript.
Independent current band PSD	Study-only calculation from recordings: Welch; Flat Top; three nonoverlapping segments; constant detrending; density scaling. Excludes the first 10 s for this comparison.
Added vibration band PSD	Research integration: Welch; Hann; two nonoverlapping segments; constant detrending; one-sided density scaling.
Vibration response	Frequency-weighted PSD integration using Equations 19–21; median across matching position recordings.
Candidate bands	2–10, 10–30, 30–100, 100–300, 300–1,000, 1,000–2,000 and 10–1,000 Hz.
Geometry	Drive end and opposite end; horizontal, vertical and axial, where available.

6.1 Diagnostic processing and independent research calculations

The review checked processing against EMPOWER 3.1. Welch is not a universal description of the technology or its diagnostic spectra. Product algorithms, internal resolution handling and correction logic are not disclosed here. The independent Welch PSD calculations in this study serve band-RMS comparison with vibration; they do not describe the proprietary diagnostic implementation.

The current-feature comparison uses the reviewed artifact treatment. Corrected feature values and the processing version must be distinguished from raw recording values in a quantitative study. The analysis does not establish correction uncertainty where physical features coincide with acquisition artifacts. Archived estimated-loss records retain an unverified processing version. The application was not changed during this review.

6.2 Selection and independence

The wider current study searched 2,373 dependent model combinations. The primary band and position were chosen after inspecting these results. Omitted-motor predictions below refit the coefficient, but they do not repeat or correct feature selection. They are an internal diagnostic, not an unbiased estimate of future accuracy. No confirmatory p-value or population confidence interval is claimed.

7 Deriving the empirical current-to-vibration formula

For positive paired measurements, let R_i be the dimensionless current-band ratio and V_i the velocity in mm/s RMS. The simplest conditional model fixes the exponent at one, $V_i \approx KR_i$. Fitting in logarithmic space gives equal weight to proportional errors rather than absolute errors. It assumes the chosen scale is appropriate and excludes zero or nonpositive inputs.

$$e_i = \ln V_i - \ln K - \ln R_i; \quad J = \Sigma e_i^2 \quad (23)$$

Set $\theta = \ln K$. Differentiating J gives $\partial J/\partial\theta = -2\Sigma(\ln V_i - \theta - \ln R_i) = 0$. Solving and exponentiating yields the geometric mean of the individual ratios:

$$K = \exp[(1/n)\Sigma \ln(V_i/R_i)] \quad (24)$$

Thus K is the fitted central multiplicative response. It is not necessarily the arithmetic conditional mean, and no lognormal mean correction is applied. K has the same units as V because R is dimensionless. Substitution of Equation 18 gives the working form:

$$V_{pred,B} = K_v 10^{DB/20}; \quad \text{for Family A, } K_v = 2.209398 \text{ mm/s} \quad (25)$$

7.1 Numerical construction of the coefficient

Motor	R_B	V mm/s RMS	V/R mm/s
A1	0.0377019	0.114387	3.033978
A2	0.0475239	0.147966	3.113502
A3	0.0372667	0.086990	2.334256
A4	0.0362795	0.058496	1.612382
A5	0.0327320	0.050315	1.537184
A6	0.0315954	0.067246	2.128336

The sum of the six log ratios is 4.75632172. Consequently, ln K = 4.75632172/6 = 0.792720287 and K = exp(0.792720287) = 2.20939846 mm/s. This calculation uses all six motors and therefore describes the fitted relationship, not an independent prediction.

7.2 Worked prediction for A1

I_B = 1.670201 A RMS and I_{ref} = 44.300178 A RMS give R_B = 0.03770191. Then $D_B = 20 \log_{10}(R_B)$ = -28.472733 dB. Equation 25 gives V_{pred} = 2.20939846 × 0.03770191 = 0.083299 mm/s RMS, compared with measured V = 0.114387 mm/s RMS. The fitted prediction is lower by a factor of 1.373.

The applicable range in these data is approximately −30.01 to −26.46 dB, at this band, family and measurement position. Extrapolation to arbitrary dB values or another motor family is unsupported.

8 Primary results and prediction checks

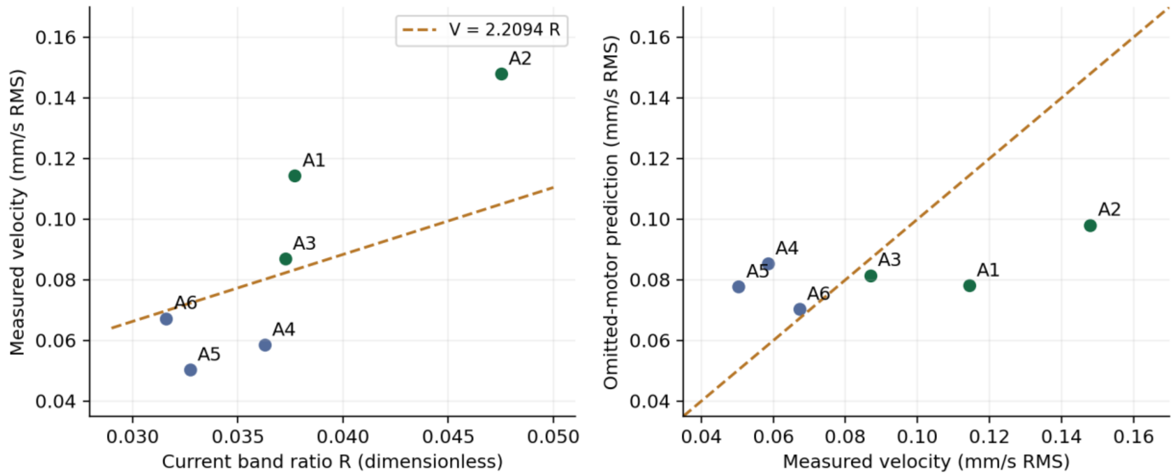

Figure 8. Family A 1–2 kHz drive-end vertical relationship. Left: all-motor proportional fit. Right: each prediction uses a coefficient refitted without that motor. Colors distinguish A1–A3 and A4–A6; neither panel is an external validation.

The log correlation between current-band ratio and velocity is 0.848516. This association is compatible with a local calibration, but it neither establishes the exponent nor identifies a shared physical disturbance. The response is broadband housing motion, not reconstructed air-gap displacement.

$$K_{-i} = \exp[(1/(n-1))\Sigma_{j\neq i} \ln(V_j/R_j)]; \quad V_{pred\,i} = K_{-i}R_i \quad (26)$$

$$F_i = \exp(|\ln(V_{pred\,i}/V_i)|) \geq 1 \quad (27)$$

Motor	D_B dB	Measured V	Omitted V_{pred}	Error factor
A1	-28.473	0.114387	0.078179	1.463
A2	-26.462	0.147966	0.098037	1.509
A3	-28.574	0.086990	0.081437	1.068
A4	-28.807	0.058496	0.085368	1.459
A5	-29.701	0.050315	0.077760	1.545
A6	-30.008	0.067246	0.070331	1.046

Velocity values in the table are mm/s RMS. The median and worst factors are 1.461 and 1.545. A factor of 1.545 means either a 54.5% overprediction or a 35.3% underprediction; it is not a symmetric ±54.5% interval. The comparison baseline predicts the geometric mean of the other motors and has median and worst factors of 1.495 and 2.048. Log-RMSE is 0.330 for Equation 25 versus 0.453 for that baseline.

The median improvement is modest. A free-exponent fit $V = CR^b$ gives $b = 2.440$ on the same six points. The imposed exponent of one is therefore a simple candidate, not an empirically established law. Separate same-band fits give $A \approx 19.4613R$ in m/s² RMS and $X \approx 0.273076R$ in µm RMS. These are separate broadband calibrations; they must not be converted into one another using an assumed band-center frequency.

9 Normalization and limits of transferability

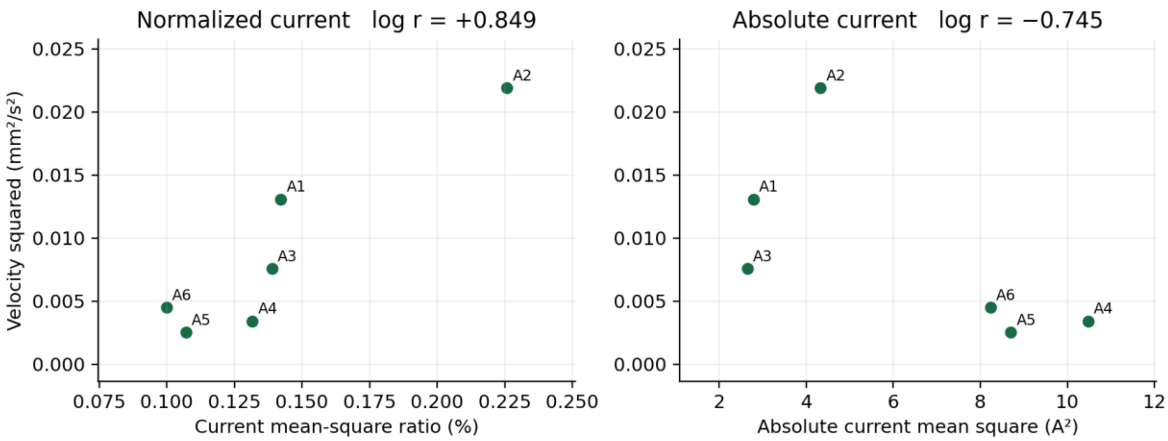

Figure 9. The same six velocity measurements compared with normalized and absolute current mean square. Normalization changes the observed association; it does not establish an energy transfer.

For Family A, the log correlation is +0.849 with normalized current mean square and −0.745 with absolute current mean square. Reference current is about 44 A in A1–A3 and 89–91 A in A4–A6. The denominator therefore contains information about the operating group. Ratios can be useful indicators while concealing absolute-current changes, an issue also emphasized in practical ESA/MCSA interpretation [15].

9.1 Grouped diagnostic

Coefficient fitted on	K mm/s	Held-out group	Median / worst factor
A1–A3	2.804164	A4–A6	1.739 / 1.824
A4–A6	1.740783	A1–A3	1.743 / 1.789

These deliberately coarse splits test portability between the observed reference-current groups. Their errors exceed the ordinary omitted-motor errors. They remain post-selection diagnostics with only three motors per group; they do not establish that load alone caused the coefficient difference. Acquisition timing, motor properties and mounting may also contribute.

9.2 Other bands and pooled evidence

A 19-motor pooled comparison at 1–2 kHz drive-end vertical has log correlation −0.113 and omitted-motor median and worst factors near 8.21 and 23.80 for a single ratio-to-velocity coefficient. Thus the Family A calibration does not generalize across the available population. Within Family A, a 300–1,000 Hz drive-end horizontal candidate has log correlation 0.884 but a worse maximum omitted-motor factor of about 3.31. Correlation alone is therefore an inadequate model-selection criterion.

The broader review did not establish a sufficiently consistent running-speed sideband relationship to justify a general formula. This is a limitation of the available acquisition and qualification evidence, not evidence that electromechanical coupling is absent. A mechanistic study should pair demodulated electrical features with the corresponding mechanical order and verify speed and load.

The load-normalized calculated diagnostic peaks in the field method can be evaluated across changing loads [4], [6], [15]. This broadband housing-amplitude regression does not test those diagnostic peaks. Its grouped prediction errors neither require equal-load MCSA comparisons nor establish a minimum diagnostic load.

9.2.1 Load changes and the meaning of signature amplitude

Load, speed and defect condition must be distinguished. Load describes the torque or power demanded by the process; speed sets mechanical repetition rates, while electrical frequency establishes the carrier and magnetic operating context. A change in raw current or housing vibration is not automatically a change in defect severity. Penrose's field publications describe calculated electrical peaks evaluated across load and speed changes [4], [6]. Equal-load comparison records are not a prerequisite for that diagnosis.

Derivation of cancellation of a common amplitude scale

For one amplitude-modulated current component, Section 3 gives $I_{sb} = mI_c/2$. Substituting into the decibel definition proves the following identity:

$$D_s = 20 \log_{10}(I_{sb}/I_c) = 20 \log_{10}(m/2)$$

If both carrier and sideband are multiplied by a common positive scale q, their ratio and D_s remain unchanged. Here q is a dimensionless amplitude multiplier, not a component disturbance coordinate. This is a mathematical explanation of how absolute current can change while relative signature amplitude remains stable. It does not assume that total motor current is proportional to shaft load, nor disclose how EMPOWER evaluates a feature.

Illustrative current scale	Carrier I_c	Sideband I_{sb}	Relative level
q = 1	2.5 A	0.010 A	−47.96 dB
q = 2	5.0 A	0.020 A	−47.96 dB
q = 4	10.0 A	0.040 A	−47.96 dB

The table assumes m = 0.008 throughout; the q values are current scales, not measured percentages of load. The sideband current quadruples while the diagnostic ratio is unchanged. These are calculated examples, not additional field observations. For the general ratio, $\Delta D_s = 20 \log_{10}(I_{sb,2}/I_{sb,1}) - 20 \log_{10}(I_{c,2}/I_{c,1})$. Thus amplitude and its reference must always be stated.

Load class determines the mechanical change

The mechanical identity $P = T\omega$ distinguishes common operating cases. For an ideal constant-torque load, doubling speed doubles power. For constant power, doubling speed halves torque. For similar centrifugal pump or fan operation at unchanged geometry and fluid density, affinity scaling gives torque proportional to speed squared and power proportional to speed cubed; doubling speed then gives four times torque and eight times power [22]. These are load laws, not universal defect-sideband amplitude laws. Efficiency changes, hydraulic operating point and process constraints can invalidate simple affinity scaling.

At a fixed speed, increased transmitted torque can change gear tooth contact, bearing contact load, belt tension and coupling forces. Whether a defect's modulation changes depends on that component and mechanism. A raw force or torque change cannot be assigned directly to a calculated electrical severity peak without its electrical relationship. Conversely, carrier-referenced field diagnosis need not be restricted to matching process loads.

For a specified tolerance P_{tol} expressed in watts, the corresponding mean torque tolerance at a shaft is $\Delta T_{tol} = P_{tol}/\omega$. At 900 r/min the factor is 0.01061 N·m/W; at 1800 r/min it is 0.005305 N·m/W. Multiply by the applicable watt tolerance; no fixed numerical tolerance is assigned here. This dimensional relationship concerns mean power and torque, not a sinusoidal spectral torque amplitude. Bearing friction, periodic modulation and magnetic pull remain separate quantities.

9.2.2 Speed changes and component frequency relationships

For a mechanical feature tied to a component, $f_m = o\,f_r$, where o is the dimensionless order and f_r is that component's shaft frequency in Hz. A simple modulated carrier gives sidebands at $f_c \pm f_m$; f_c is the electrical carrier frequency. When speed or electrical frequency changes, the calculated locations change accordingly. A bearing or gear feature is not required to remain at one fixed FFT frequency. For an induction-machine slip-related feature, the relevant separation follows slip and supply frequency rather than one universal shaft order [4], [6], [15].

Component or condition	Frequency relation	Amplitude and operating effects
Rotor magnetic asymmetry and UMP	Static/dynamic patterns involve the electrical carrier, shaft speed and rotor geometry.	Electrical evidence concerns magnetic asymmetry. Housing response also depends on force direction and structural response. Geometric rotor displacement is not required for every signature [4], [18].
Rolling-element bearings	Characteristic orders depend on bearing geometry and the speed of the bearing shaft.	Contact load, clearance, lubrication and the loaded zone affect local mechanical response. ESA/MCSA can reflect radial and torsional effects; copying a high-frequency vibration envelope into current analysis is not the field method [4], [6], [23], [24].
Gears and couplings	Gear mesh = tooth count × gear shaft frequency; defects can modulate mesh or shaft-related patterns.	Transmitted torque affects tooth loading and contact. Gear ratio relates the component speeds. Torque and magnetic coupling provide system evidence; housing vibration depends on the local path [4], [6].
Belts and pulleys	Pulley orders and belt circulation depend on actual speeds and belt geometry.	Tension, slip and radial bearing load can change independently of speed. Use the actual component relationship; no single amplitude exponent covers all belt faults.
Pumps and fans	Vane/blade passage = count × shaft frequency; process instabilities need their own relation.	Hydraulic/aerodynamic load and operating point affect forces and torque modulation. Mean affinity-law power is not a prediction of a cavitation or vane-sideband dB value [22], [25].
Reciprocating components	Cycle orders follow crank speed and the number and sequence of working events.	Pressure, valve condition and loading sequence affect the torque waveform. A speed change moves cycle frequencies; a pressure change can alter amplitudes without changing speed.

For example, an illustrative bearing order of 4.8 moves from 72 Hz at 900 r/min to 144 Hz at 1800 r/min. A 24-tooth gear on those shafts moves from 360 to 720 Hz mesh frequency. These examples establish frequency location only; they do not predict defect size, current dB, or housing acceleration. Rolling-element slip and contact-angle changes can perturb ideal bearing orders [24].

For a fixed RMS displacement $X = 1$ µm at one shaft order, $V = 2\pi fX$ and $A = (2\pi f)^2X$ give $V = 0.09425$ mm/s and $A = 0.008883$ m/s² at 15 Hz; at 30 Hz they become 0.18850 mm/s and 0.03553 m/s². Velocity rises 6.02 dB and acceleration 12.04 dB relative to their respective first values even though displacement is unchanged. This is a kinematic proof under a fixed-displacement assumption, not a universal speed law for a defect.

9.2.3 What the derivation and field evidence establish

The radial and torsional models in Sections 2.5–2.6 connect a physical disturbance to different measured responses. Even if a carrier-referenced electrical signature stays unchanged with load, the vibration-to-current coefficient can change with speed because the housing transfer function is evaluated at a different frequency. Location, direction, mounting and the selected vibration quantity remain part of that coefficient.

The force-to-vibration calculation

For the single-mode housing model, the magnitude of the displacement response is:

$$|x_h| = |F| / \sqrt{(k - m\omega^2)^2 + (c\omega)^2}$$

Below resonance, stiffness dominates and $|x_h| \approx |F|/k$. Above resonance, inertia dominates and $|x_h| \approx |F|/(m\omega^2)$. Near resonance, damping controls the peak. If rotating mass unbalance provides |F| proportional to ω^2, displacement grows approximately as ω^2 in the stiffness-dominated region but approaches a constant in the inertia-dominated region. The same fault therefore does not have one universal speed exponent across a resonance. These limiting cases follow from the stated model; they are not fitted transfer functions of the field machines.

For UMP, the pressure relationship $p_n \approx B^2/(2\mu_0)$ gives $\delta p_n \approx B\delta B/\mu_0$. Its circumferential distribution determines the net force, as shown in Section 2.5.1. Neither load percentage alone nor a measured vibration magnitude supplies B, δB or the spatial distribution. Magnetic signatures and housing motion should therefore be related through the mechanism rather than by treating current dB as a direct force measurement.

Field evidence and the scope of the proof

Evidence	What it establishes	What it does not establish
Penrose practical DFIG application [4]	Reports platform-dependent PPF/dynamic-eccentricity amplitudes that do not depend on load; calculated locations follow operating frequency.	A single universal amplitude coefficient for every machine platform or every housing axis.
Penrose DFIG powertrain paper [6]	Describes carrier-referenced spectra and field identification of radial and torsional component relationships.	A controlled amplitude-versus-speed surface for each bearing, gear and pump condition.
Penrose wedge/coil field cases [5]	Inspected defects and repair evidence support magnetic detection without requiring a strong UMP-driven mechanical response.	A universal equivalence between electrical severity and local vibration amplitude.
Present paired field comparison	Six-machine numerical fit and omitted-machine checks for the stated band and sensor location.	An independently controlled load × speed × defect-severity experiment. The fitted coefficient is not proof of all component mechanisms.

The mathematical proofs establish ratio cancellation, frequency movement and conditional mechanical scaling. The cited field work supports practical diagnosis during operating changes. To establish a quantitative vibration conversion surface for a component, independently vary speed, process load and confirmed condition, retain individual vibration axes and evaluate the corresponding calculated electrical peaks. That is a validation design for the proposed conversion formula, not a requirement for routine single-CT MCSA diagnosis.

9.3 Comparison for mechanical fault detection

The comparisons below prioritize field applications [1], [2], [3], [4], [5], [6]. MCSA is the first system assessment for the electric machine scope; the final column describes the targeted follow-up needed for each diagnostic objective. Detecting a condition, identifying its source and quantifying a local motion are different tasks. The field amplitude regression was not evaluated as a fault classifier.

Issue	Vibration evidence	MCSA evidence	Preferred use and limitation
Rolling-element bearing damage	Local acceleration, envelope spectra and repeated impacts can reveal bearing-related periodicity.	Radial field and air-gap torque modulation identify bearing and lubrication condition, including driven bearings [4], [6].	MCSA first for system diagnosis; targeted vibration/enveloping for local impact response. The two detect different consequences of bearing condition.
Unbalance	Running-speed radial response plus phase and speed dependence [26].	May appear through radial gap modulation or associated loading.	Vibration with phase for balancing and localization. A current feature alone does not locate the heavy spot; 1× is not unique to unbalance.
Misalignment	Axial/radial response, phase and harmonics provide evidence [26].	Can alter torque and air-gap signatures; weak components require leakage control [20].	Vibration plus alignment measurement to confirm geometry. MCSA can diagnose coupled train condition, but neither a 2× peak nor a current sideband is unique.
Looseness and soft foot	Location-dependent harmonics, impacts and changed response under loading [26].	May become visible if mounting changes field symmetry or torque.	Vibration across feet/housings and mechanical inspection. An electrical response can indicate consequences without identifying the loose interface.
Structural resonance	Large response, phase change and spatial mode pattern as excitation frequency changes.	Can show the exciting disturbance, but not automatically identify the structural mode.	Vibration with speed sweep or frequency-response testing. A strong current feature and a strong vibration feature can have different causes.
Gear damage	Mesh-related vibration, modulation and local transient signatures.	Field applications identify gearbox stages and bearing modulation through the air-gap response [4], [6].	MCSA first for the coupled train; local vibration for structural response and localization. High-frequency vibration attenuation is not a limit on torque-based diagnosis.

Envelope analysis is a separate processing method: it demodulates a selected vibration resonance band to reveal impact repetition. The present acceleration/velocity/displacement band-RMS study does not implement or benchmark that method. Its 1–2 kHz result must not be treated as a test of early bearing detection capability.

9.4 Electrical faults and coupled system disturbances

Issue	Vibration contribution	MCSA or ESA contribution	Preferred use and limitation
Broken rotor bars or rotor-circuit asymmetry	Can reveal resulting force or speed modulation.	Current patterns near $f_s(1 \pm 2s)$ and related components provide established evidence; s is slip [27].	MCSA evaluates calculated peaks during changing load/speed; adequate resolution separates the relevant features. Lower-load rotor limits depend on resolving close pole-pass peaks, not a fixed minimum load percentage.
Stator winding or converter-related stress	May show secondary electromagnetic-force vibration.	Current/voltage patterns can reveal electrical changes; Penrose reports winding-stress applications [1].	ESA and appropriate electrical confirmation. Current alone cannot establish insulation strength or exclude supply/control effects.
Air-gap eccentricity or magnetic asymmetry	Directional motion and magnetic-force response help evaluate mechanical effects.	Slot-related and modulation patterns can reveal electromagnetic asymmetry [10], [18], [27].	Use both: current for magnetic signature, vibration for motion and localization. Physical rotor offset is not the only possible explanation.
Voltage imbalance or harmonic excitation	Can show resulting force response and resonant amplification.	Voltage and current together distinguish supply excitation from the observed current response.	Power-quality/ESA measurements first; vibration assesses mechanical consequence. Current-only attribution to the supply is incomplete.
Torsional or driven-load oscillation	Housing motion is indirect unless the torsional-to-housing path is known.	Small air-gap torque changes produce current signatures without requiring measurable speed ripple [2], [6].	MCSA for coupled torsional-condition diagnosis; shaft-angle/speed or torque sensing for direct torsional confirmation. Neither gives housing amplitude without a transfer model.
Cavitation or hydraulic instability	Pump-local vibration reveals structural response to fluid excitation.	Specialized current features can detect cavitation-related load changes [28].	MCSA first for system assessment; targeted vibration and process measurements distinguish hydraulic duty and structural consequences.

These comparisons support combining the technologies rather than treating “omnidirectional” as a guarantee that current is more sensitive to every fault. MCSA integrates radial and torsional effects that couple into the electromagnetic response. Vibration resolves motion along a selected axis at a selected point. Their strengths are complementary precisely because their transfer paths differ.

9.5 What the additional literature establishes

Thomson and Fenger present industrial current-signature applications for rotor bars, stator turns and eccentricity [27]. Calculated rotor sidebands depend on slip; adequate resolution is needed when they lie close to the carrier. This supports fault-specific electrical analysis; it does not supply a universal dB-to-vibration conversion or justify assigning every nearby sideband to rotor damage.

Sun et al. (2024) use noise reduction and signal decomposition to extract current indicators of cavitation in a controlled pump study [28]. Their reported improvements concern their processing and tested conditions. They do not establish that an arbitrary MCSA band-RMS value outperforms local vibration for all pumps. Sun et al. (2026) use inverse frequency-response analysis of vibration from two pumps and find condition-dependent sensitive bands [25]. This provides a particularly relevant demonstration that the structural transfer function affects which frequency band appears informative.

Bruinsma et al. publish paired current, voltage and vibration data for induced faults in motor-driven pumps, including bearing, rotor, winding, mounting, alignment and hydraulic conditions [29]. This is a useful candidate for a future controlled comparison. The dataset article establishes availability and acquisition design, not a winner between modalities. Its waveforms were not analyzed for this manuscript.

Selecting a measurement for the diagnostic objective

Objective	Most defensible starting approach
Locate a local mechanical source	Vibration at multiple relevant points and directions, using waveform, spectrum, phase or envelope features appropriate to the fault.
Diagnose coupled motor/driven equipment	MCSA first: one CT and one acquisition. Use component frequencies and modulation relationships; targeted follow-up resolves a specific ambiguity.
Separate electrical excitation from mechanical response	Synchronized voltage, current and vibration, with actual speed and operating context.
Quantify shaft torsional vibration	Angular position/speed or torque measurements, or an independently identified electrical model. Housing acceleration alone is not a twist measurement.
Predict housing vibration from current dB	A location-, direction-, frequency- and condition-specific calibration, tested on independent acquisitions.
Assess mechanical condition and energy	ESA with operating duty and a calibrated torque/loss model can estimate mechanical energy effects. Input/output power establishes total loss; component allocation needs additional evidence.

A fair comparative study should predefine defect labels and severity, acquisition bandwidth, processing, operating envelope and decision thresholds. It should report false alarms and missed detections separately from amplitude-prediction error, and reserve entire motors or sessions for testing. Published performance figures from different rigs and algorithms cannot be ranked as if they were one controlled experiment.

9.6 Visual guide to choosing the measurement

For electric machine systems, including changing-load and variable-speed operation, begin with MCSA: one current clamp, on one phase, with one two-minute acquisition provides a simultaneous view of coupled motor and driven-component condition [4], [6]. Use the resulting frequency relationships to direct follow-up work. Calculated-peak evaluation does not require equal-load records. Add vibration for local motion, direction, structural amplification, balancing or localization. Add voltage/current ESA when power quality, transformer interaction or measured active power is required.

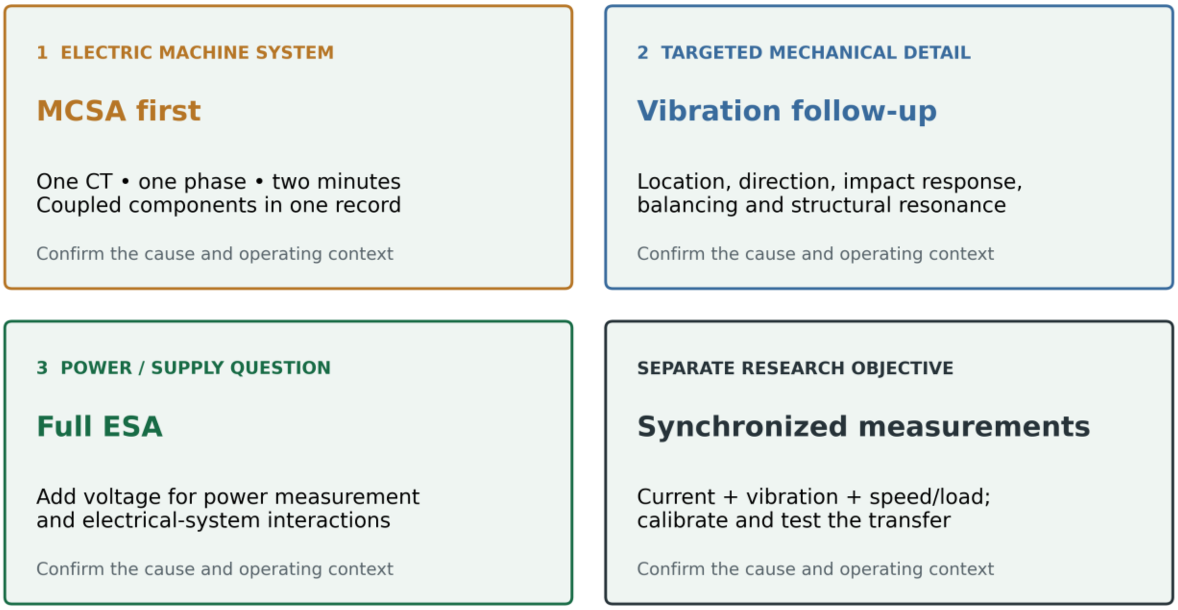

Figure 10. Practical measurement choices. MCSA is the first system assessment for the electric machine scope. Targeted vibration and full ESA answer subsequent questions. The separate research task of calibrating current to vibration requires paired measurements.

A simple example of complementary evidence

Suppose a bearing housing shows high vertical vibration while a current signature also increases. The vibration change may be amplified by a support resonance, while current may reflect radial field modulation, torsional load variation or an electrical change. Agreement strengthens the case for investigating the system, but does not prove that the current and vibration amplitudes have one common cause or a fixed ratio.

Identifying relationships between system components

MCSA can identify relationships between components through their shared electrical response: shaft-speed ratios, gear-mesh and belt frequencies, load cycles and modulation patterns can link a driven component to motor radial or torsional behavior [2], [4], [6]. For example, a gear-mesh component with sidebands spaced at a known shaft speed can associate the modulation with that stage of the train. Component speeds, ratios and characteristic modulation patterns support interpretation within the same acquisition; targeted follow-up can resolve a specific ambiguity. This is system-level diagnostic information, not simply a motor-only fault reading. Coincident peaks alone do not establish causality; quantitative transfer gains require identification, and several sources may share a frequency.

10 Mechanical component condition and watt losses

Mechanical condition affects mean torque, radial force and torsional ripple. MCSA/ESA supports mechanical-condition diagnosis and calibrated loss estimation across bearings, gears, couplings, belts, seals and rubbing interfaces. Vibration helps locate impacts and structural response; the useful measurement depends on the diagnostic objective.

Measured or estimated watt losses usually include general friction and other losses, not only losses caused by degradation or defects. Normal rolling and sliding friction, seals, lubricant drag and windage can contribute even in serviceable equipment. An electrical system boundary may also include copper, core and drive losses. Total loss is therefore distinct from the incremental loss attributable to a condition change; the latter requires a stated reference and an appropriate loss allocation.

10.1 Bearing and transmission loss mechanisms

Bearing and driven-component changes can affect the electrical signature through radial and torsional interaction. Quantitative loss estimates should state their applicable tolerance in watts, P_{tol}, for the machine, operating range and estimation method. No fixed watt value or universal detection floor is assigned in this manuscript. A tolerance is a specified allowable deviation; it is distinct from the standard uncertainty u_P of an estimate and from the smallest condition change that can be detected. These quantities require their own supporting evidence and must not be treated as interchangeable.

SKF separates bearing frictional moment into rolling, sliding, seal and lubricant-drag contributions [23]. Their relative importance changes with loading, speed and lubrication. This motivates a condition-dependent model, rather than assigning one watt value to a bearing-frequency peak:

$$M_f = M_{rolling} + M_{sliding} + M_{seal} + M_{drag} \quad (28)$$

Loss models account for radial and axial load, preload, alignment, clearance, wear, lubricant state and seals. Belt tension and misalignment can increase bearing loading; gears and churning add losses. Strong local impacts do not necessarily imply large mean drag, while smooth friction can consume watts with weak discrete spectral lines.

Penrose’s field application papers identify generator and driven bearings, lubrication-related signatures, gearing and rotor/stator conditions through electrical analysis [4], [6]; his ASM chapter provides additional application context [30]. Laboratory lubrication studies [31], [32] support friction and signal-processing models but do not take precedence over these field capabilities. Mechanical condition must be included when interpreting estimated watt losses, even when local high-frequency impact vibration is small.

10.2 Mean resistance and periodic disturbance are distinct

$$\langle P\rangle = \langle T\omega\rangle = \bar{T}\bar{\omega} + \langle \tilde{T}\tilde{\omega}\rangle \quad (29)$$

Here T is torque across a specified rotating interface in N·m and ω is angular speed in rad/s; bars denote means and tildes denote zero-mean fluctuations. The expression assumes a stationary averaging interval. Torque and speed must refer to the same interface and sign convention. For resolved sinusoidal components, the fluctuation term is:

$$\langle \tilde{T}\tilde{\omega}\rangle = \Sigma_h \, T_{h,RMS} \, \Omega_{h,RMS} \cos \varphi_h \quad (30)$$

φ is the torque–speed phase difference. Oscillation amplitude alone omits phase and can represent stored and returned energy. At nearly constant speed, steady friction raises mean power without necessarily producing a large sideband. Current also responds to radial field modulation.

10.3 From condition to an estimated watt value

$$P_{friction} = M_f\omega = (2\pi/60)nM_f \quad (31)$$

With speed n in r/min and frictional moment M in N·m, power is in watts. If moment is supplied in N·mm, the multiplier becomes 2π/60000 = 0.0001047198. This is a dimensional conversion of identified friction torque, not a direct conversion of spectral decibels [23].

Worked bearing-condition example — illustrative inputs

Assume a bearing operates at 1,800 r/min and an independently identified friction model gives 0.20 N·m in the reference condition and 0.35 N·m in the changed condition. Angular speed is 188.4956 rad/s. The corresponding losses are 37.699 W and 65.973 W; the estimated increase is 28.274 W. These assumed torques are not observations from the field motors. The example shows how lubrication, loading or wear can enter a watt calculation through a calibrated condition-to-friction model.

$$\Delta P_{friction,est} \approx \bar{\omega}\,\Delta M_{f,est} \quad (32)$$

For a resolved current feature, an independently identified torque/current gain can instead estimate a periodic torque component:

$$T_{h,est} = |G_{Ti,h}|\, I_{ref} 10^{Dh/20} \quad (33)$$

The gain has units N·m/A and must include the feature definition, modulation mechanism, load, control behavior and frequency response. This expression applies to a calibrated component, not automatically to a broad current band. Radial and torsional contributions must be separated or represented jointly. Combining its result with measured speed ripple and phase can estimate power transfer at that frequency; it does not recover mean friction from sideband amplitude alone.

Electrical balance and component allocation

$$P_{in} = \langle \Sigma_{phases}\, v(t)i(t) \rangle \quad (34)$$

At steady state, electrical input equals useful output plus all losses inside the chosen system boundary [33], [34]. For energy attribution, a duty-adjusted before/after component-loss change can be estimated as the input-power change minus useful-output change and changes in all other losses. Those other losses include load-dependent copper loss, core and drive losses, and other mechanical components. Input watts alone establish aggregate demand, not its allocation to one bearing.

Thus current-only MCSA can classify condition and support a calibrated estimate; voltage/current ESA adds active-power evidence. Torque/speed measurements, process output, temperature and a validated component model strengthen attribution. A current-derived torque estimate must be validated against a suitable reference before its watt accuracy is claimed.

10.4 Vibration energy and condition-aware comparisons

Mean-square quantities remain useful when their physical coordinates are specified. R^2 is a normalized electrical mean-square ratio, not an input-power fraction; housing acceleration squared is not dissipated power.

$$\langle E_k \rangle = ½ m_{eff} V^2; \quad P_d = cV_{rel}^2; \quad P_{mech} = \langle Fv \rangle \quad (35)$$

The first expression assumes an effective mass moving at RMS velocity V. The second assumes a viscous damper and relative velocity across it, in SI units. The third is translational mechanical power. Housing motion alone identifies neither mass nor damping [16]. Balanced winding copper loss is approximately $P_{cu} = 3\Sigma_h R_{ac,h} I_{ph,h}^2$, using actual phase currents and operating resistance. These relationships complement the rotating-interface energy balance; they are not interchangeable loss estimators.

10.5 Archived-estimate comparisons

Archived estimated-loss values L were matched to exact current recordings, with duplicate analyses represented by a median. Their algorithm version and absolute scale were not independently established. They were not regenerated under the reviewed 3.1 loss workflow. The following relationships therefore compare an algorithm-dependent estimate with measured vibration; they do not close an energy balance.

Scope	Local fitted relationship	Log r	Worst amplitude factor
Family A; n = 6; 10–30 Hz; drive-end horizontal	V ≈ 0.0449586√L	0.771	1.278
Family B; n = 4; 10–1,000 Hz; drive-end vertical	A ≈ 0.287496√L	0.952	1.174

L is the numerical archived estimate in kW; V is mm/s RMS and A is m/s^2 RMS. The coefficients carry the corresponding amplitude per √kW units. The error factors are coefficient-refitted omitted-motor results. These leads were selected from 3,780 dependent comparisons and remain especially fragile at n = 4. Squaring both positive variables leaves their logarithmic correlation unchanged and supplies no independent confirmation.

10.6 Worked estimate and baseline extension

For an illustrative L = 3.00 estimated kW within the Family A range, $V^2 = 0.0020212745 \times 3 = 0.006063824$ mm^2/s^2, so V = 0.0778706 mm/s RMS. This predicts the local comparison response only. It does not show that 3 kW is dissipated in the measured structure or recoverable through maintenance.

$$y^2 - y_o^2 \approx \alpha(L - L_o); \quad y \approx \sqrt{[y_o^2 + \alpha(L - L_o)]} \quad (36)$$

Equation 36 is a baseline-aware candidate for future matched-duty tests. A comparable noise/background model for the primary relationship would be $y^2 \approx y_o^2 + K^2R^2$ if independent contributions justify addition of mean squares. The current dataset does not independently identify those background terms.

10.7 Capabilities reconsidered and validation design

Objective	Role of current / ESA	Role of vibration and confirmation
Bearing impact or surface damage	Radial and torsional signatures can support fault identification when coupling and resolution are adequate.	Local acceleration/envelope, multiple locations and bearing geometry help locate impact sources.
Lubrication, drag and excessive loading	Mean torque/load features plus current patterns can support condition classification; calibrated models estimate frictional demand.	Vibration and temperature constrain condition; load, viscosity, lubricant quantity and speed constrain loss.
Gear, belt and coupling condition	Coupled torque and radial effects support diagnosis across the train; ESA can assess changes in aggregate electrical demand.	Local vibration, alignment/tension checks and process data distinguish competing sources.
Maintenance energy benefit	Matched-duty ESA plus useful-output and other-loss corrections estimates the change attributable to intervention.	Mechanical confirmation identifies what changed; shaft torque/power or validated loss models test the estimate.

A loss-model validation test pairs current, voltage, vibration, speed and temperature before and after a documented mechanical intervention, with process output and operating state accounted for in the loss balance. These are energy-attribution controls, not conditions required for MCSA defect detection. Record bearing designation, loads, lubricant state and component geometry where available. Estimate both mean-loss change and periodic features, retain their uncertainty, and reserve independent operating points for validation. A bearing or transmission model can supply an estimated watt value even without a direct component torque sensor, provided its assumptions and validation range are stated.

The present anonymous dataset has no independently verified bearing-condition labels or matched maintenance interventions. Condition differences are therefore plausible explanatory variables for coefficient variation, not established diagnoses of Families A or B. The archived loss comparisons remain useful exploratory leads, but they cannot validate the new friction model or establish recoverable energy savings.

11 Uncertainty and validation requirements

11.1 Propagation of scale and frequency uncertainty

For a resolved component V = A/(2πf), small independent relative uncertainties satisfy approximately $(u_V/V)^2 = (u_a/A)^2 + (u_f/f)^2$. For $X = A/(2\pi f)^2$, the frequency contribution becomes $4(u_f/f)^2$. These expressions omit covariance and spectral-estimation bias; they are not uncertainty estimates for the present data. Actual instrument tolerances were not independently available.

$$dV_{pred}/V_{pred} \approx dK/K + (\ln 10/20)dD \quad (37)$$

With K held fixed, a +1 dB change gives a factor $10^{1/20} = 1.1220$, whereas −1 dB gives 0.8913. Coefficient uncertainty, acquisition mismatch and selection error must be added to this dB sensitivity. A common current gain cancels in a band/reference ratio only if it acts identically on numerator and denominator. Vibration calibration directly scales K; frequency-dependent response does not generally cancel.

11.2 A confirmatory experiment

For validation of the proposed quantitative current-to-vibration formula, freeze the feature, coordinate, processing and acceptance criterion before new acquisition. Paired current/vibration sessions and independent test motors are research controls for estimating K and its transferability. They are not requirements for routine MCSA diagnosis: the operational method addressed here uses one CT, one phase and one two-minute acquisition. Additional voltage, speed or temperature measurements serve the specific validation or power-attribution question.

Compare the fixed-exponent model with a constant baseline, a free-exponent model and a baseline-aware mean-square model. Select any new features only within training data, using nested validation if necessary. Report errors by motor and operating condition, confidence intervals based on independent units, and raw-versus-corrected sensitivity. For a proposed physical mechanism, test the corresponding carrier-demodulated current feature against the mechanical order; raw same-frequency correlation is insufficient.

12 Conclusion

The most defensible simple relationship is $y \approx K10^{D/20}$, conditional on a stated current reference, response quantity, frequency feature, motor family and operating envelope. For the selected six-motor example, $V \approx 2.2094 \times 10^{DB/20}$ mm/s RMS describes the 1–2 kHz drive-end vertical comparison. The arithmetic is reproducible, but its predictive value is preliminary and its coefficient is sensitive to grouping and normalization.

Exact spectral and kinematic identities provide the calculation framework. Literature supports the existence of electromechanical coupling; it does not validate this field coefficient. The pooled failure, free-exponent result and grouped checks delimit the claim. A synchronized, pre-specified experiment is the next step toward a transferable amplitude relationship. MCSA/ESA also supports mechanical-condition diagnosis and condition-aware loss estimates through both mean torque demand and radial/torsional modulation. Watt attribution requires a calibrated torque/loss model or an appropriate power balance; the archived fits do not yet provide that validation.

For practical electric machine assessment, the reviewed field evidence supports MCSA first: one CT, one phase and one two-minute acquisition. Calculated radial and air-gap torque peaks identify component relationships during changing load, speed and frequency without equal-load comparison records. Resolution governs close-peak load limits; targeted vibration resolves local motion [2], [4], [6].

References

[1] H. W. Penrose, "Evaluation of stator and rotor interturn stress with electrical signature analysis in variable frequency drive and wind generator applications," in *Proc. IEEE Electr. Insul. Conf. (EIC)*, 2020, pp. 274–277, doi: 10.1109/EIC47619.2020.9158738.

[2] H. W. Penrose, "Evaluation of DFIG wind turbine generator and transformer conditions with electrical signature analysis," in *Proc. IEEE Electr. Insul. Conf. (EIC)*, 2022, pp. 379–384, doi: 10.1109/EIC51169.2022.9833161.

[3] H. W. Penrose, "Insulation system reliability in wind generation," in *Proc. IEEE Electr. Insul. Conf. (EIC)*, Seattle, WA, USA, 2015, pp. 358–361.

[4] H. W. Penrose, "Practical application of electrical and current signature analysis in DFIG turbine systems," application manuscript, n.d.

[5] H. W. Penrose, "Evaluation of asynchronous wind generator stator magnetic slot wedge and coil movement using electrical signature analysis," in *Proc. IEEE Electr. Insul. Conf. (EIC)*, 2021, pp. 1–4, doi: 10.1109/EIC49891.2021.9612312.

[6] H. W. Penrose, "The application of electrical and current signature analysis for DFIG turbine and powertrain defects," in *Proc. IEEE Power Energy Soc. Gen. Meeting (PESGM)*, 2025, pp. 1–4, doi: 10.1109/PESGM52009.2025.11225587.

[7] M. Blödt, P. Granjon, B. Raison, and G. Rostaing, "Models for bearing damage detection in induction motors using stator current monitoring," *IEEE Trans. Ind. Electron.*, vol. 55, no. 4, pp. 1813–1822, 2008, doi: 10.1109/TIE.2008.917108.

[8] F. Immovilli, A. Bellini, R. Rubini, and C. Tassoni, "Diagnosis of bearing faults in induction machines by vibration or current signals: A critical comparison," *IEEE Trans. Ind. Appl.*, vol. 46, no. 4, pp. 1350–1359, 2010, doi: 10.1109/TIA.2010.2049623.

[9] F. Immovilli and M. Cocconcelli, "Experimental investigation of shaft radial load effect on bearing fault signatures detection," *IEEE Trans. Ind. Appl.*, vol. 53, no. 3, pp. 2721–2729, 2017, doi: 10.1109/TIA.2016.2633236.

[10] S. Zhang *et al.*, "Model-based analysis and quantification of bearing faults in induction machines," *IEEE Trans. Ind. Appl.*, vol. 56, no. 3, pp. 2158–2170, 2020, doi: 10.1109/TIA.2020.2979383.

[11] Brüel & Kjær, *Mechanical Vibration*, technical handbook. Accessed: Sep. 12, 2026. [Online]. Available: https://www.bksv.com/media/doc/bn1330.pdf

[12] PCB Piezotronics, "Guidelines for mounting test accelerometers." Accessed: Sep. 12, 2026. [Online]. Available: https://www.pcb.com/resources/technical-information/mounting

[13] Fluke, "Triaxial vs. single-axis sensors: Are they equivalent?" Accessed: Sep. 12, 2026. [Online]. Available: https://www.fluke.com/en-us/learn/blog/vibration/triaxial-vs-single-axis-sensors-are-they-equivalent

[14] C. Kar and A. R. Mohanty, "Monitoring gear vibrations through motor current signature analysis and wavelet transform," *Mech. Syst. Signal Process.*, vol. 20, no. 1, pp. 158–187, 2006, doi: 10.1016/j.ymssp.2004.07.006.

[15] H. W. Penrose, "Examining load effects on ESA/MCSA and the importance of resolution," *RELIABILITY Magazine*. Accessed: Sep. 12, 2026. [Online]. Available: https://reliamag.com/articles/load-effects-on-esa-mcsa/

[16] COMSOL, "Frequency response of mechanical systems," *COMSOL Blog*, 2019. Accessed: Sep. 12, 2026. [Online]. Available: https://www.comsol.com/blogs/frequency-response-of-mechanical-systems

[17] D. H. Staelin, "Actuators and sensors, motors and generators," in *Electromagnetics and Applications*, MIT OpenCourseWare, course 6.013, Spring 2009, ch. 6. Accessed: Sep. 12, 2026. [Online]. Available: https://ocw.mit.edu/courses/6-013-electromagnetics-and-applications-spring-2009/e163397146247bc4558e1acfa8ff74d2_MIT6_013S09_chap06.pdf

[18] H. W. Penrose, "Electrical signature analysis air-gap eccentricities (Part I): Static and dynamic eccentricity," *The RAM Review*, Nov. 8, 2020. Accessed: Sep. 12, 2026. [Online]. Available: https://theramreview.com/electrical-signature-analysis-esa-air-gap-eccentricities-part-i-static-and-dynamic-eccentricity/

[19] L. Huang, G. Shen, N. Hu, L. Chen, and Y. Yang, "Coupled electromagnetic-dynamic modeling and bearing fault characteristics of induction motors considering unbalanced magnetic pull," *Entropy*, vol. 24, no. 10, Art. no. 1386, 2022, doi: 10.3390/e24101386.

[20] N. Afrizal and R. Ferrero, "Leakage error compensation in motor current signature analysis for shaft misalignment detection in submersible pumps," *IEEE Trans. Instrum. Meas.*, vol. 69, no. 11, pp. 8821–8830, 2020, doi: 10.1109/TIM.2020.2998301.

[21] National Instruments, "FFT power spectrum and PSD for 1 chan VI," *LabVIEW API Reference*. Accessed: Sep. 12, 2026. [Online]. Available: https://www.ni.com/docs/gd-GB/bundle/labview-api-ref/page/vi-lib/measure/maspectr-llb/fft-power-spectrum-and-psd-for-1-chan-vi.html

[22] U.S. Department of Energy, *Improving Motor and Drive System Performance: A Sourcebook for Industry*, Sep. 2008. Accessed: Sep. 12, 2026. [Online]. Available: https://www1.eere.energy.gov/manufacturing/tech_assistance/pdfs/motor.pdf

[23] SKF, *Rolling Bearings*, catalogue 17000 EN. Accessed: Sep. 12, 2026. [Online]. Available: https://www.skf.com/binaries/pub12/Images/0901d196802809de-Rolling-bearings---17000_1-EN_tcm_12-121486.pdf

[24] SKF, "Vibrations help find faulty components," *Evolution*. Accessed: Sep. 12, 2026. [Online]. Available: https://evolution.skf.com/us/vibrations-help-find-faulty-components-3/

[25] Y. Sun *et al.*, "Experimental investigation of cavitation excitation characteristics of centrifugal pump based on load spectrum identification," *Measurement*, vol. 260, Art. no. 119771, 2026, doi: 10.1016/j.measurement.2025.119771.

[26] SKF, *Spectrum Analysis*, technical guide CM5118 EN. Accessed: Sep. 12, 2026. [Online]. Available: https://www.skf.com/binaries/pub12/Images/0901d1968024acef-CM5118-EN-Spectrum-Analysis_tcm_12-113997.pdf

[27] W. T. Thomson and M. Fenger, "Current signature analysis to detect induction motor faults," *IEEE Ind. Appl. Mag.*, vol. 7, no. 4, pp. 26–34, 2001, doi: 10.1109/2943.930988.

[28] H. Sun, Q. Lan, Q. Si, N. Chen, and S. Yuan, "Cavitation detection via motor current signal analysis for a centrifugal pump in the pumped storage pump station," *J. Energy Storage*, vol. 81, Art. no. 110417, 2024, doi: 10.1016/j.est.2024.110417.

[29] S. Bruinsma, R. D. Geertsma, R. Loendersloot, and T. Tinga, "Motor current and vibration monitoring dataset for various faults in an E-motor-driven centrifugal pump," *Data Brief*, vol. 52, Art. no. 109987, 2024, doi: 10.1016/j.dib.2023.109987.

[30] H. W. Penrose, "Electrical and motor-current signature analysis," in *ASM Handbook*, vol. 18, *Friction, Lubrication, and Wear Technology*. ASM International, 2017, pp. 1040–1044, doi: 10.31399/asm.hb.v18.a0006430.

[31] M. Lopez-Ramirez, R. J. Romero-Troncoso, D. Morinigo-Sotelo, O. Duque-Perez, D. Camarena-Martinez, and A. Garcia-Perez, "Discriminating the lubrication condition from the rotor bearing fault in induction motors using Margenau-Hill frequency distribution and artificial neural networks," *Ind. Lubr. Tribol.*, vol. 69, no. 6, pp. 970–979, 2017, doi: 10.1108/ILT-08-2016-0177.

[32] F. de Cadier de Veauce *et al.*, "Power losses of oil-bath-lubricated ball bearings—A focus on churning losses," *Lubricants*, vol. 12, no. 11, Art. no. 362, 2024, doi: 10.3390/lubricants12110362.

[33] Natural Resources Canada, *Electric Motors: Energy Efficiency Reference Guide*. Accessed: Sep. 12, 2026. [Online]. Available: https://natural-resources.canada.ca/energy-efficiency/energy-star/electric-motors-energy-efficiency-reference-guide

[34] Yokogawa, "Electric motor power measurement and analysis." Accessed: Sep. 12, 2026. [Online]. Available: https://www.yokogawa.com/uk/library/resources/media-publications/electric-motor-power-measurement-and-analysis/

[35] H. W. Penrose, "Application of electrical signature analysis," SUCCESS by DESIGN, technical application paper, n.d. Accessed: Sep. 12, 2026. [Online]. Available: https://www.motordoc.org/wp-content/uploads/2019/01/Application-of-Electrical-Signature-Analysis.pdf

[36] H. W. Penrose, "An understanding of induction motor performance through electrical signature analysis—Part 1," MotorDoc LLC, white paper, 2024. Accessed: Sep. 12, 2026. [Online]. Available: https://empathcms.com/wp-content/uploads/2024/05/An-Understanding-of-Induction-Motor-Performance-through-Electrical-Signature-Analysis-Part-1.pdf

[37] H. W. Penrose, "Evaluating wind turbines with electrical signature analysis," *NETA World J.*, Aug. 2024. Accessed: Sep. 12, 2026. [Online]. Available: https://netaworldjournal.org/2024/08/howardwpenrose/emerging-technologies/evaluating-wind-turbines-with-electrical-signature-analysis/

[38] ALL-TEST Pro, "Power plant," application case study, n.d. Accessed: Sep. 12, 2026. [Online]. Available: https://alltestpro.com/wp-content/uploads/2019/07/Power-Plant-English.pdf

[39] SKF Technical Support, "Configuring the spectrum envelope alarm in SKF @ptitude Analyst." Accessed: Sep. 12, 2026. [Online]. Available: https://skftechnicalsupport.zendesk.com/hc/en-us/articles/360039753354-Configuring-the-Spectrum-Envelope-Alarm-in-SKF-ptitude-Analyst

Literature review scope

The six supplied papers [1], [2], [3], [4], [5], [6] were reviewed in full and take precedence for practical capability and workflow. Field inspection, repair and commissioning evidence is distinguished from illustrative models. References [7], [8], [9], [14], [20], [25], [26], [27], [28], [29] were reviewed through available abstracts, previews or indexed passages, not a complete full-text review. Reference [10] and available Penrose sources [1], [18], [35], [36], [37] were examined in the earlier review. Technical guidance [11], [16], [17], [21], [23], [26], [33], [34], [38], [39] supplies measurement context. Sources [30], [31], [32] support application or friction-model context at the previously available abstract/indexed-text level. None independently validates the present amplitude coefficients or archived watt estimates. Watt tolerances remain application-specific and are not established numerically by this dataset. References [12], [13] were reviewed as manufacturer application guidance, not independent validation of the fitted coefficient. Reference [19] supports the UMP mechanism; sources [22], [24] support load laws and bearing-frequency interpretation. All figures are original schematics or anonymized plots; the review is targeted rather than systematic.

Appendix A Calculation audit and reproducibility

The direct-fit coefficient, all six omitted-motor predictions, constant baseline, free slope and grouped diagnostics were recalculated for this revision. Independent re-integration of the six cached current spectra and corresponding vibration spectra reproduced the primary current-band magnitudes and motor-level velocity values within a relative numerical tolerance of 10^{-10}. The ten vibration responses underlying the secondary loss comparisons were previously independently recalculated from the original vibration recordings, including calibration, filtering and PSD integration, and agreed within the same tolerance. This establishes numerical consistency, not independent sensor or model validation.

Audit item	Result / interpretation
Direct velocity coefficient	2.2093984566 mm/s; geometric mean of six V/R ratios.
Direct log correlation	0.8485156327.
Direct omitted-motor errors	Median 1.461258; maximum 1.545460.
Constant baseline errors	Median 1.495391; maximum 2.047831.
Free log–log exponent	2.440119; fixed exponent 1 is an imposed model choice.
Grouped coefficients	2.804164 and 1.740783 mm/s; operating-group sensitivity remains.
Secondary squared coefficients	0.0020212745 for Family A; 0.0826538271 for Family B, in stated units.
Inventory and anonymity	20 matched motors; 116 motor-side recordings; neutral identifiers throughout.

A.1 Minimum reproduction record

Retain the original waveform, calibration parameters, current reference and its frequency, sample rate, start-time removal, segment length, window, PSD normalization, research preprocessing version. Record each band boundary and sensor position, per-record response, motor-level aggregation and exact train/test allocation. Rounded manuscript values reproduce the displayed results to their reported precision; full retained precision was used for fitting.

A.2 Availability and unresolved items

Customer identities, acquisition paths and raw recordings are omitted from this manuscript. The six anonymized primary feature pairs are provided in Section 7. Raw data access and a redistributable reproduction package would need to be arranged before a journal submission requiring them. Author attribution and correspondence are listed on the cover. Contributions, funding and conflict-of-interest declarations require confirmation before submission; no such declarations are inferred here.

Absolute calibration certification, exact operating load and speed, the archived loss-estimator version, correction uncertainty at overlapping physical and acquisition features, and independent predictive performance remain unresolved. MotorDoc LLC and HRI Labs identify the requested manuscript context; no external peer review, journal acceptance or third-party certification is asserted.

Appendix B Equipment capabilities and reading-time estimates

The charts on the final three pages summarize the principal capabilities across common equipment. They are an engineering synthesis of Sections 2, 9 and 10, not a claim that every fault is detectable with every instrument. All driven-equipment MCSA entries assume an electrically coupled motor or generator and a sufficiently strong radial or torsional path. Electrical measurements can diagnose coupled mechanical condition as well as electrical condition; vibration adds spatial and directional information.

B.1 What the collection times include

Vibration times are illustrative route estimates including sensor positioning, recording and a quick quality check. Routine MCSA uses one current clamp on one phase and one 2-minute acquisition for the coupled system [6]. Setup at an accessible feed is quick. No repeated acquisition, second phase or visit to each mechanical component is assumed. Travel, access preparation, process waiting, interpretation and reporting are outside both estimates. These are planning times rather than measured route throughput.

Timing element	Vibration	MCSA
Routine acquisition assumption	5–20 s per point/direction or simultaneous channel set; 15–30 s for repositioning and quality checks.	One current clamp; quick setup at an accessible feed. Fixed 2 min per data collection.
Basis of train estimate	Two bearing sites × three axes = six channels: six sequential single-axis acquisitions or two simultaneous triaxial acquisitions.	One current clamp at one feed per independent motor; one collection can include several coupled components.
Resolution and operation	Low-frequency response, averaging and changing speed can alter the vibration acquisition/interpretation plan.	One 120 s record in this comparison. Diagnostic load limits depend on resolved calculated peaks; changing load/speed does not itself require repeats.
Installed sensors	Parallel channels can substantially reduce operator time; record duration still sets frequency detail.	Installed current sensors reduce connection time; voltage channels are additionally required for measured active power.

Illustrative route: 12 single-axis acquisitions × (10 s recording + 20 s positioning/checking) = 6 min; four simultaneous triaxial acquisitions × 30 s = 2 min. The chart's VIB ranges assume sequential readings. MCSA uses one 2 min collection [6]. SKF guidance [39] supports vibration route context. Full ESA and phase comparison are separate scopes.

B.2 Resolution dependent load limits

Diagnostic load limits depend on the effective resolution needed to distinguish the calculated peaks; they are not a universal minimum percentage of rated load. At lower induction-motor slip, rotor-related sidebands move closer to the carrier, making their separation the relevant question [6], [15]. Changing load, speed or frequency does not itself prevent MCSA diagnosis or require equal-load comparison records. The evaluated frequencies follow the operating condition.

For a generic contiguous record, $1/T_{rec}$ gives nominal Fourier spacing: 120 s corresponds to 0.00833 Hz [6]. Actual feature separation also depends on window bandwidth and signal conditions. This standard identity is not a specification of EMPOWER's internal processing or its feature-specific acceptance criteria. The independent research band integration in Section 6 must not be used to infer the product's diagnostic limits.

B.3 Measurement points and earliest defect evidence

A vibration location is a physical bearing housing or other selected structural point. The chart assumes horizontal, vertical and axial readings at each accessible location: 4 locations × 3 axes means 12 channel readings, not 12 separate housings. A triaxial sensor with simultaneous acquisition records those axes together at one site; its channels are not automatically equivalent to single-axis sensors at different housing locations (Section 2.2.2). Point counts are a starting route for the stated equipment configuration, not a guaranteed minimum for every diagnosis; extra bearings, feet, gearbox stages or inaccessible interfaces change the requirement.

The MCSA comparison uses one CT on one phase, at one accessible electrical point, for one two-minute acquisition. It does not require multiple phases or repeated measurements. The same record supports identification of radial and torsional relationships among coupled components [4], [6]. Vibration point count grows with the locations and directions visited; MCSA does not add a clamp or a reading for each bearing or gearbox stage. Full voltage/current ESA is a distinct scope for measured power and broader electrical-system assessment.

Early detection is a condition threshold, not a fixed countdown

The chart describes the earliest plausible observable evidence under suitable conditions. It does not assign weeks or months before failure. The time from first detectable change to functional failure depends on failure mode, growth rate, duty, sensor path, processing, thresholds and inspection interval. Abrupt failures may provide little warning. The six-motor amplitude study contains no dated defect-onset or failure observations from which to estimate lead time.

For localized rolling-element damage, appropriately selected acceleration/envelope features can reveal small impacts before overall velocity increases. MCSA can reveal small electrical asymmetry and coupled radial/torsional changes; lubrication or friction-related loading may change without a strong impact signature [4], [6]. Neither sequence is universal. A claim that one method detects a defect earlier requires simultaneous observation of the same defect under the same duty, with predefined thresholds and comparable false-alarm rates.

Estimating a defensible lead time in a future study

Record the first sustained threshold crossing separately for each method, the confirmed defect condition, inspection interval and an independently defined intervention or functional-failure endpoint. The elapsed interval from detection to that endpoint is observed warning time, with uncertainty from sampling and any censoring by maintenance. Do not interpret amplitude or correlation alone as remaining useful life. A shorter acquisition improves route efficiency; it does not by itself establish earlier defect detection.

Capability statements below are a mechanism-based synthesis of the cited literature and Sections 2, 9 and 10. Equipment-specific early-stage statements are conditional engineering expectations, not validated sensitivity or lead-time benchmarks. Times follow B.1: one CT, one phase, one 2-minute acquisition. Specialized investigations require a separate acquisition plan.

The chart includes changing-load and variable-speed equipment. Evaluate calculated peaks at the applicable speed and electrical frequency without requiring equal-load comparison records. Resolution-dependent close-peak limits must be stated for the selected processing path; retain one CT and one acquisition in this routine comparison.

B.4 Motors pumps fans and belt drives

Capability, earliest plausible evidence, measurement points and estimated minutes per train including changing load and speed. MCSA assumes 2 min per collection; see B.1–B.3. Early evidence is not a guaranteed warning interval.

Equipment	Vibration capability / earliest evidence	MCSA capability / earliest evidence	VIB points / time	MCSA points / time
AC motor, direct coupled	Bearing impacts; unbalance; alignment response; looseness; resonance; location and direction. **Early:** Small bearing impacts may emerge in a suitable envelope band before overall vibration rises.	Rotor/stator asymmetry; eccentricity; radial and torsional mechanical signatures; friction/load changes. **Early:** Small electrical asymmetry or coupled radial/torque changes can precede gross symptoms.	2 sites 6 readings **2–5 min**	1 feed 1 current clamp **2 min**
Centrifugal pump and motor	Motor/pump bearings; alignment; impeller or vane response; hydraulic excitation and cavitation. **Early:** Local bearing impacts or hydraulic changes can appear before gross performance loss.	Motor electrical condition; coupled pump loading, vane/torque modulation and validated cavitation indicators. **Early:** Hydraulic load changes or coupled defects may appear at onset if their current signature is resolved.	4 sites 12 readings **4–15 min**	1 feed 1 current clamp **2 min**
Fans and blowers	Unbalance, deposits, blade-pass response, bearings, looseness and structural resonance. **Early:** Developing unbalance or local bearing impacts can precede severe vibration.	Motor condition; coupled blade/load variation, radial effects and drag changes; context needed to identify source. **Early:** Coupled blade/load or electrical changes can appear before severe mechanical symptoms.	4 sites 12 readings **4–15 min**	1 feed 1 current clamp **2 min**
Belt-driven equipment	Pulley alignment, belt-related response, local bearings, looseness and driven-shaft vibration. **Early:** Belt-order or local bearing changes can precede major slip or mechanical damage.	Belt/load modulation; tension-related radial loading and drag; motor condition. Slip/tension needs confirmation. **Early:** Tension-related loading or periodic torque changes may precede gross slip; attribution needs confirmation.	4–6 sites 12–18 readings **5–20 min**	1 feed 1 current clamp **2 min**

Vibration readings assume three axes at each site. MCSA assumes one current clamp, not one sensor per mechanical component. Use suitable bandwidth and characteristic-frequency interpretation. A historical baseline supports trending but is not a prerequisite for a single-record MCSA diagnosis.

B.5 Gearboxes compressors conveyors and process drives

Capability, earliest plausible evidence, measurement points and estimated minutes per train including changing load and speed. MCSA assumes 2 min per collection; see B.1–B.3. Early evidence is not a guaranteed warning interval.

Equipment	Vibration capability / earliest evidence	MCSA capability / earliest evidence	VIB points / time	MCSA points / time
Gearbox and motor	Gear mesh, modulation, impacts and bearing condition; localization by measurement point. **Early:** Mesh modulation or repeated impacts can reveal localized damage before large overall vibration.	Gear/load torsional modulation and motor condition; radial effects where coupled. Transmission varies with frequency. **Early:** Weak coupled modulation can precede gross damage; field reports include early gearbox and bearing condition [4], [6].	4–8 sites 12–24 readings **5–20 min**	1 feed 1 current clamp **2 min**
Rotary compressor or chiller	Bearings, alignment, rotor/mesh or screw-passing response, rubs and structural excitation. **Early:** Local bearing/rotor features may change before broad vibration or performance alarms.	Motor condition; compression/load modulation, coupled bearing/rotor condition and abnormal demand. **Early:** Coupled load/rotor changes may precede gross loss; evaluate calculated peaks as load and speed change.	4–8 sites 12–24 readings **5–20 min**	1 feed 1 current clamp **2 min**
Conveyor and geared drive	Drive bearings, gearing, pulley/roller defects near sensors and structural response. **Early:** Local roller/bearing impacts can precede seizure if those locations are measured.	Drive electrical condition, coupled gear/belt loading, periodic drag and jam/load changes; component relationships follow the coupled torque path. **Early:** Drag or periodic loading can precede a jam; identify the roller or drive relationship from its characteristic modulation.	4–8 sites 12–24 readings **5–25 min**	1 feed 1 current clamp **2 min**
Mixer, agitator or extruder	Bearings, gearing, alignment, shaft/support response and local mechanical impacts. **Early:** Local bearing/gear features can precede gross symptoms; variable process forcing can mask them.	Motor condition, process torque cycles, coupled drivetrain faults and drag; viscosity/duty can resemble faults. **Early:** Torque-cycle or drag changes may appear early, but process viscosity/load is a competing cause.	4–8 sites 12–24 readings **5–20 min**	1 feed 1 current clamp **2 min**

For conveyor estimates, the route covers the drive assembly; surveying all idlers adds points and time. Gear stages and process cycles must be mapped to actual shaft speeds. MCSA can associate component relationships through coupled modulation, with operating context used to confirm the source.

B.6 Vertical pumps reciprocating machines and generators

Capability, earliest plausible evidence, measurement points and estimated minutes per train including changing load and speed. MCSA assumes 2 min per collection; see B.1–B.3. Early evidence is not a guaranteed warning interval.

Equipment	Vibration capability / earliest evidence	MCSA capability / earliest evidence	VIB points / time	MCSA points / time
Vertical or submersible pump	Accessible motor/head bearings, structural modes and transmitted pump response; submerged localization limited. **Early:** Early local damage may be visible at accessible bearings; remote submerged impacts can be attenuated.	Motor electrical and coupled pump condition from accessible feed; hydraulic/mechanical source requires corroboration. **Early:** Electrical or coupled hydraulic/mechanical changes may precede gross symptoms despite poor local access.	2–4 sites 6–12 readings **4–15 min**	1 feed 1 current clamp **2 min**
Recip. compressor or pump	Cycle-related impacts, looseness, bearing and valve-response evidence with timing reference. **Early:** Cycle-resolved impact or valve-response changes may precede large overall vibration.	Cycle torque/loading asymmetry and motor condition; cylinder or valve attribution needs phase/process evidence. **Early:** Cycle-load asymmetry may precede broad alarms when timing and normal load patterns are known.	6–10 sites 18–30 readings **10–30 min**	1 feed 1 current clamp **2 min**
Centrifuge or separator	Rotor unbalance, bearing damage, rubs, looseness and speed-dependent resonance. **Early:** Developing unbalance or local bearing impacts can precede broad alarms.	Motor condition, coupled torque/radial changes and loading; calculated peaks are evaluated at the applicable speed/frequency. **Early:** Coupled radial/torque or electrical changes may precede gross symptoms; changing load and speed are within the diagnostic scope.	4–6 sites 12–18 readings **5–20 min**	1 feed 1 current clamp **2 min**
Generator or wind turbine train	Local bearing/gear condition, alignment, structure and rotor dynamics where instrumented. **Early:** Local bearing/mesh features can precede broad alarms with suitable sensors and operating bins.	Generator bearings, rotor connections, wedges, gearbox and main-bearing condition [4], [6]. **Early:** Developing rotor impedance, wedge or lubrication signatures can support intervention before gross failure.	6–12 sites 18–36 readings **10–30 min**	1 feed 1 current clamp **2 min**

Generator entries use electrical-signature principles with machine- and converter-specific models. An unmotorized asset has no applicable motor-current signal. Oil analysis, ultrasound, offline insulation tests and geometry checks provide capabilities outside these two methods. Current-derived watt estimates need calibration; measured active power requires voltage and current.

Appendix C A simple explanation of motor testing

A simple guide to vibration and electrical clues

A motor uses electricity and magnets to turn a shaft. That shaft can run a fan, pump or other machine. If a part wears out, it can change the shaking, the electricity, or both. We can look for these clues before the machine stops working.

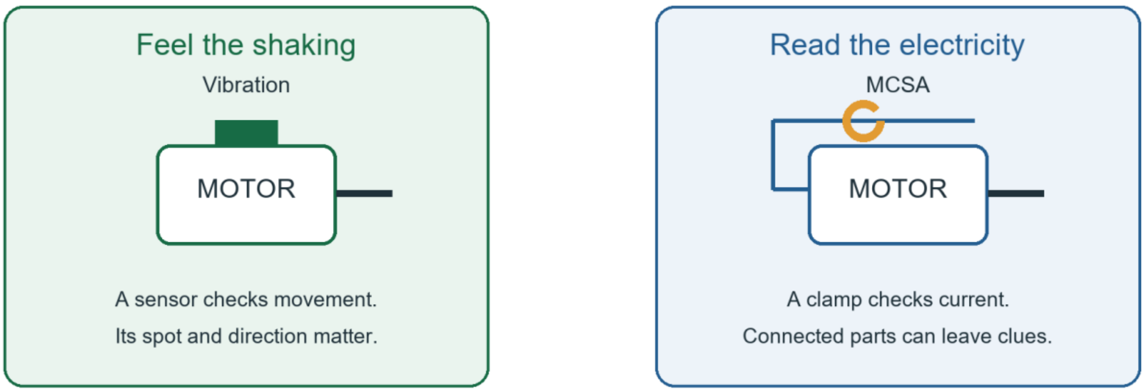

Figure 11. Two ways to find clues. Vibration senses local movement; MCSA reads electrical changes associated with the motor and coupled components.

One way feels movement

Vibration testing measures tiny shakes. A sensor sits on the machine, often near a bearing. A bearing helps a shaft turn smoothly, much like the bearings in a skateboard wheel.

Another way checks electricity

MCSA means motor current signature analysis. Current is the flow of electricity. A trained person puts a special clamp around one wire and records it. For the method in this guide, one recording takes two minutes. Parts connected to the motor can leave clues in that recording, too.

ESA means electrical signature analysis. It can also use voltage measurements. Voltage is like the push that moves electricity. Those extra measurements can help answer more electrical questions.

What the Numbers Mean

Imagine a playground swing moving back and forth. Three numbers can describe its motion.

Displacement

How far it moves from its middle position.

Velocity

How fast it moves, and in which direction.

Acceleration

How quickly its velocity changes as it speeds up, slows down or turns around.

Frequency tells us how many back-and-forth movements happen each second. A small, fast shake can have a large acceleration even when it barely moves. So we must know both the size of the motion and how fast it repeats.

What does dB mean

Decibels, written dB, are a way to compare sizes. In this current test, a small electrical clue is compared with the main electrical signal. It is not a measurement of how loud the motor sounds. We must know what the dB number is being compared with.

Why there is no magic conversion number

A dB value cannot turn straight into a shaking value for every machine. The part, speed, kind of shake and sensor position all matter. The paper studies a simple rule:

Estimated shaking = electrical clue size × a matching number

Here, "electrical clue size" is a ratio found from the dB value. A ratio compares the clue with the main signal. The "matching number" is worked out from measurements. It only applies to the kind of comparison for which it was checked.

Pretend the clue ratio is 0.01 and the matching number is 2 millimeters per second. The estimate is 0.02 millimeters per second. This is a made-up example to show the multiplication, not a rule for every motor.

Why Both Ways Are Useful

Magnets can pull unevenly

There is a narrow gap between the motor's turning part and its fixed part. If the magnetic pulls around that gap do not balance, the motor has unbalanced magnetic pull. This can affect shaking and leave electrical clues. Changes in the twisting force can leave clues, too. The motor does not have to slow down enough for us to notice.

The sensor spot matters

A vibration sensor feels movement at its own spot. A loose cover or a path through several joints can weaken or change a clue. Other shaking can hide it. A sensor that checks one direction may miss motion going another way. A three-axis sensor checks three directions at once, but still only at that spot.

Speed and work are different

Speed means how fast a shaft turns. Load means how much work the machine is being asked to do. Think of pedaling a bicycle: pedaling faster is a speed change; climbing a hill makes the work harder.

Faster rotation can move a clue to a different frequency. More work can change the amount of current. If the little clue and the main signal both double, their ratio stays the same. The method described in the paper can find faults while speed and load change. Matching loads and repeated recordings are not required for its normal check.

Start with the whole system then look closer

For the electric machines covered here, MCSA is a quick first check of the motor and connected parts. Vibration testing helps show where movement is happening and in which direction. Together, they give different pieces of the same puzzle.

The paper found a useful possible link in one small group of motors. That does not prove one conversion rule works for every machine. More testing is needed to check that rule.

Based on the technical manuscript by Howard W. Penrose, Ph.D., CMRP
MotorDoc LLC and HRI Labs • info@motordoc.com
12 September 2026